Master's thesis
Astronomy

Comparing the magnetically active young star V889 Herculis to the Sun

Teemu Willamo

October 26, 2017

Supervisor: doc. Thomas Hackman

Examiners: prof. Karri Muinonen
doc. Thomas Hackman

UNIVERSITY OF HELSINKI
Department of Physics

PL 42 (Gustaf Hällströmin katu 2a)
00014 Helsingin yliopisto

“The cosmic law of gravity

Pulled the newborns around a fire

A careless, cold infinity

In every vast direction”

—The Greatest Show on Earth, by Nightwish

HELSINGIN YLIOPISTO — HELSINGFORS UNIVERSITET — UNIVERSITY OF HELSINKI

Tiedekunta — Fakultet — Faculty	Laitos — Institution — Department
Faculty of Science	Department of Physics

Tekijä — Författare — Author
Teemu Willamo

Työn nimi — Arbetets titel — Title

Comparing the magnetically active young star V889 Herculis to the Sun

Oppiaine — Läroämne — Subject
Astronomy

Työn laji — Arbetets art — Level	Aika — Datum — Month and year	Sivumäärä — Sidoantal — Number of pages
Master's thesis	October 26, 2017	66

Tiivistelmä — Referat — Abstract

This Master's Thesis deals with stellar magnetic activity, both as it is seen in the Sun, our closest star, and in other, more extreme examples of stellar activity. For the Sun, much higher quality data is available, and for a much longer time, so it remains by far the best studied star, although stars, that are much more magnetically active, have been discovered. This thesis will review the most common forms of magnetic activity, as observed both in the Sun and in other stars. A special focus is given to BY Draconis -type stars. These are young stars, whose photometric brightness variations are caused by large, cool starspots, similar to the sunspots seen on the Sun.

A particular BY Draconis -star, V889 Herculis, is analysed in detail, using spectroscopic and photometric methods. From spectroscopy, by the Doppler imaging method, a surface temperature map can be constructed for the star. From photometry, both short-term and long-term variations of the star can be studied. During the 20 years time span of the photometric data, the star seems to have gone through similar activity cycles as the well known 11 year solar cycle.

The aim of this thesis is to compare solar and stellar activity in general, and specifically V889 Her to the Sun. Based on the analysis, the basic properties of V889 Her, seen in previous studies, are confirmed: a large polar spot is present on its surface, and there are clear changes in its activity. As the stellar parameters, like mass and surface temperature, of V889 Her are very similar to the Sun, and it is also a single star, the main difference is age. As a young star, V889 Her is still magnetically much more active than the Sun today, but probably it will continue to become more and more similar to the present Sun, losing its high activity with increasing age. Similarly, V889 Her shows us what the Sun most likely was like billions of years ago.

Avainsanat — Nyckelord — Keywords
Stellar magnetic activity, Sunspots, Doppler imaging, Continuous Period Search, V889 Herculis

Säilytyspaikka — Förvaringsställe — Where deposited

Muita tietoja — övriga uppgifter — Additional information

Acknowledgements

First of all, I would, of course, like to thank my supervisor, Doc. Thomas Hackman, who always took the time to answer my questions, more or less related to the topic of this thesis, when needed. If I ever felt like getting lost in the careless, cold infinity known as stellar magnetic activity, I knew I had someone to guide me forward.

I also want to thank Prof. Ilya Usoskin, from the University of Oulu. Twice I had the chance of working as a summer trainee in Oulu, where I learned what scientific work really is in practice, and our collaboration has continued even past that. The work I did regarding sunspot numbers has also been directly applicable to this thesis. I am also very grateful for being included in several publications based on the work I did, even as the main author!

Another very helpful person deserving my gratitude is Dr. Jyri Lehtinen, who would always have some answer to my questions. Besides answering many questions about active stars, Jyri has also guided me in the use of the Observatory of Metsähovi, for which there is one figure as proof even in this thesis.

I have also to thank all my friends studying physics and astronomy with me during these years. We have taught much to each other, perhaps even more so than any of the teachers. Especially Joonas and Akke, thanks for all the discussions related to astronomy, or any other topics for that matter. And for the nights spent in Metsähovi. The nights spent there are among the best ones in my life. Seriously, what is the point of astronomy, if you never get to see the wonders of the night sky yourself?

Finally, my thanks goes to my parents, Ripa and Sasu, who supported me in every manner during the writing of this thesis and the way towards a scientific career. Especially Ripa must also be mentioned for many advices related to my studies, as that is your job not only as a parent, but also at the University.

Contents

1. Introduction

Stellar magnetic activity is observed in many different forms. Sunspots were seen already by the medieval Chinese on the surface of the Sun. The modern scientific observations of sunspots started in the early 17th century, shortly after the introduction of the telescope. They have been recorded and counted regurlarly ever since, forming one of the longest time series of astronomical data.

Physically, sunspots are cooler areas on the visible surface of the Sun, the photosphere, and thus appear dark in comparison to their surroundings. They often form groups of multiple spots. Schwabe (1844) was the first to notice a periodic cycle, approximately with the length of 11 years, in the number of sunspots, some times referred to as the Schwabe cycle. The exact length of the cycle, however, varies with a few years from cycle to cycle.

The sunspot number remains by far the longest direct time series of stellar activity, spanning for over 4 centuries. The series has been expanded back in time through measurements of decaying radioactive isotopes, most commonly ^{14}C and ^{10}Be, stored in natural archives such as tree rings and ice layers in glaciers, which can be independently dated. These can be used as a proxy of solar activity, because their abundance depends on the flux of galactic cosmic rays reaching the Earth's atmosphere, which in turn is strongly reduced by solar activity. The isotopes are formed through spallation reactions caused by collisions with the cosmic rays. This way the series has been indirectly extended to span for over 10000 years (Usoskin et al., 2007).

Other indicators used for solar activity include the total sunspot area, the F10.7 index (flux of 10.7 cm radio waves), the flare index (measuring energy released by solar

flares), the coronal index (strength of the Fe XIV coronal emission line) and Ca II H&K indices (strength of the Ca II H&K emission lines), which all follow a more or less similar periodicity (Usoskin, 2013).

Similar activity has been found in other stars as well. Stellar activity is an important area of research, because it is a major part of stellar evolution, but also because a general understanding of stellar activity helps us understand the Sun, and how changes in our closest star might affect life on Earth.

In addition to dark sunspots, the amount of brighter faculae also increases during high activity. Whereas spots in all stars have a reducing effect on the luminosity, simultaneously appearing faculae brighten the star. In the Sun, the effect of faculae dominate over the darkening of sunspots, which leads to the total irradiance of the Sun being highest during solar activity maxima. In other, more active types of stars, spots are so large that they dominate the total luminosity of the star, leading to reduced luminosity during activity maxima (Radick et al., 1990).

In many stars, the spot activity is concentrated on certain, long lived active regions, which stay on a constant longitude. These are called active longitudes. Whether active longitudes exist in the Sun is a question, which has been much discussed (e.g. Berdyugina and Usoskin, 2003; Pelt et al., 2005).

Whereas the sunspot number series spans for over 400 years, and indirect proxies for solar activity reach thousands of years back, photometric time series of other active stars span only for a few decades. This has allowed the discovery of similar periodic cycles as the solar cycle, but the data for other stars is still very limited when compared to the Sun. Also shorter variations, caused by rotation, can be seen in the light curves, because the spot distribution on the stellar surface is not homogenous. The Continuous Period Search -method (CPS) is used in this thesis to study these effects.

With very few exceptions, surfaces of stars other than the Sun cannot be resolved directly, so generally no direct proof exist that the changes in luminosity are caused by starspots. However, through an indirect method, called Doppler imaging, the distribution of surface temperature on magnetically active stars can be mapped, thus resolving spots. This is done by tracking distortions in the spectral lines of the star. These are caused

by temperature differences on the surface, and can be detected if the star rotates rapidly enough, thus widening the lines through the Doppler effect. By combining Doppler imaging to time series analysis, a more extensive view of magnetic activity can be achieved.

All the phenomena described above probably arise from changes in the stellar magnetic field, which is generated by a dynamo operating inside the star, as ionized plasma moves in the convective zones, driven by convection and rotation. The full solar magnetic cycle is roughly 22 years (referred to as the Hale cycle, in contrast to the Schwabe cycle), including a change in polarity on average every 11th year, which is seen as an 11 year variation in the sunspot number.

These phenomena will be studied in the data of V889 Herculis, a magnetically active young solar analogue, belonging to the BY Draconis -class of variables. Photometric time series analysis and spectroscopic Doppler imaging will be applied to study the object, comparing it to historical data of the Sun. The fundamental research question would be, what similarities and differences there are between the activity of a young solar-like star like V889 Her and the present Sun.

The thesis is structured as follows: in chapter 2 the basic observations and theory of solar and stellar magnetic activity in its different forms are presented. Especially BY Draconis -stars are discussed more in detail, and also other phases in the evolution of solar-like stars are mentioned. Chapter 3 presents the methods used in the data analysis: Doppler imaging and time series analysis, which concentrates particularly on the Continuous Period Search -method. Chapter 4 presents the object of this study, V889 Her, and what is known about this star from previous studies, as well as the photometric and spectroscopic data used. In chapter 5, the results of applying the methods to the data, are presented. Finally, chapter 6 summarizes the thesis, and discusses the main conclusions drawn from the analysis.

2. Stellar magnetic activity

2.1 Sunspots

Sunspots, small, dark spots on the solar surface, are perhaps the best known form of stellar magnetic activity. Hale (1908) was the first one to observe the existence of magnetic fields in sunspots, measured from the Zeeman effect on spectral lines. Hale's continued observations revealed that spots, when found in pairs, which is quite common, usually have different magnetic polarity, where the leading spot (with reference to the direction of the Sun's rotation) is closer to the equator than the trailing spot. The polarities of these pairs are reversed on the other hemisphere, so that the meridional component of the field is pointing in the same direction (north or south) on both hemispheres, following the global solar magnetic field, which more or less resembles a dipole field (see section (2.3.5) for a more complete description of the global field). The polarity of the whole solar magnetic field changes every solar cycle (Hale and Nicholson, 1925).

Sunspots are seen as darker areas on the solar surface because their temperature is lower than that of their surroundings. They are formed due to loops in the magnetic field rising radially through the surface of the Sun. The strong magnetic field diminishes convection, so plasma cannot rise efficiently from the interior, hotter layers to the surface. Spots often form in pairs or larger groups around the magnetic loops. Since the magnetic field is 'sourceless', a field line rising through the surface must go back at some point. As the field line rises through one spot, it is a natural thought that it dives back to the solar interiors in the spot's pair. This is often the case, and quite striking magnetic loops can be formed in between, where plasma easily gets trapped, revealing the magnetic structure (figure 2.1). This gives a quantitative way to define a spot group, as the spots belonging

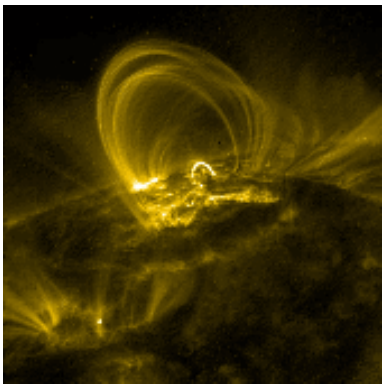

Figure 2.1: A coronal loop in the Sun, imaged by NASA's Transition Region and Coronal Explorer spacecraft (TRACE).

to the same magnetic loop. Of course, by means of visual observations only, it can be difficult to determine which spots are magnetically connected to each other, if there is no data of the polarity of the spots. In some cases spots belonging to the same group can be separated from each other by great distances. However, it is not uncommon to find an isolated spot with uniform polarity; in these cases, the magnetic field goes back through the solar surface at an invisible spot, which can be seen only through magnetic observations (Hale and Nicholson, 1925). In rare cases the spot might be strictly unipolar; then the field lines symmetrically surround the spot or group of spots with uniform polarity, and emerge back through the photosphere through flocculi spread around the spot (Hale and Nicholson, 1925).

The temperature in the photosphere of the quiet Sun (solar surface without significant activity) is around 5800 K, whereas sunspots are around 4500 K. The centre of a sunspot is called umbra, which is darker and cooler than the surrounding penumbra. Both the umbra and the penumbra are visible in the largest sunspots in figure (2.2). The magnetic field in the umbra is approximately radial, compared to the more inclined field in the penumbra.

Although spots in other stars can be resolved by Doppler imaging, resolving the umbra from the penumbra is difficult because of the poorer angular and temperature resolution. Nevertheless, large spot sizes and temperature contrasts suggest that the spot is dominated by the umbra. With smaller spot sizes and temperature contrasts the

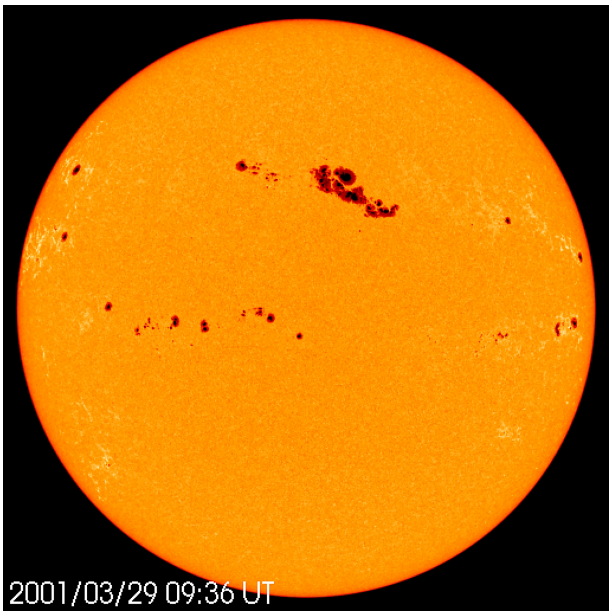

Figure 2.2: The Sun close to activity maximum, imaged by NASA's SOlar and Heliospheric Observatory (SOHO). Multiple spots and spot groups can be seen on the surface. Also the penumbra surrounding the darker umbra can be seen around the largets spots.

penumbra would be expected to dominate the variations (Berdyugina, 2005).

Typical life times of sunspots vary from days to months. In some stars, spots, or at least active regions forming constantly new spots, can last considerably longer, for years or even decades. Also the spot size varies: sunspots cover typically an area from a few to a few hundred millionths of the solar disk (msd), the largest measured sunspot group being over 6000 msd, as measured 8.4.1947 by the Royal Greenwich Observatory[1]. Scaling these with the actual size of the Sun, we see that the physical size of sunspots is comparable to that of the Earth. The largest known starspots, on the other hand, can cover over half of a hemisphere and be larger than the entire Sun (Strassmeier, 1999). However, because of the limitations in resolving stellar spots, it is very difficult to tell whether one is observing a single, large spot, or an extensive group of spots.

A commonly used indicator of stellar spot activity is the filling factor f_s, which gives the fraction of the stellar disk covered by spots. In active stars this can reach values of over 0.5 (O'Neal et al., 1998), which means that over half of the hemisphere visible to us is covered by spots. In the Sun, during solar maxima, the total sunspot area reaches only

[1]Data available at http://solarscience.msfc.nasa.gov/greenwch.shtml

values of a few thousandths of the solar disk. In the stellar case, however, the resolution is much poorer. Small spots, with sizes comparable to sunspots, might easily go undetected. Thus the stellar filling factors are not completely reliable, and could in reality be even larger (Solanki and Unruh, 2004). However, as stellar spots and spot groups are difficult to distinguish, large areas with small spots might appear as one huge spot, in which case the spot filling factor would be overestimated. Therefore it is not straightforward, whether the estimated stellar filling factor tends to be too high or too low.

Sunspots are typically concentrated around the equator, between latitudes of about 30 degrees north and south (see figure 2.6). Starspots, on the other hand, have been observed even on polar areas (such is the case, for instance, with V889 Herculis, the object of this study). Because the complete absence of these in the Sun, there has to be some fundamental difference in the mechanisms producing these spots. In very active, rapidly rotating stars the occurence of polar spots has been explained by the coriolis force deflecting rising magnetic flux tubes in the convective zone towards the poles (Schüssler and Solanki, 1992), or by the meridional flow transporting magnetic field close to the surface to the poles (Schrijver and Title, 2001). Some discussion has been aroused about whether these polar spots are a real phenomenon, or if they could be artefacts, (e.g. Bruls et al., 1998). This issue is regarded more in detail when discussing the faults of the Doppler imaging -method in chapter (3.1).

2.2 Rotation

Stellar magnetic fields are believed to arise from dynamo effects inside the star. The effects are governed by forces moving the plasmas in the stellar interior: rotation and turbulent convection. Unlike convection, which takes place inside the star, rotation is easy to observe, and will be discussed more in detail.

Magnetic activity anticorrelates with the Rossby number:

$$Ro = \frac{P_{\mathrm{rot}}}{\tau_{\mathrm{conv}}}, \tag{2.1}$$

where P_{rot} is the rotational period and τ_{conv} the convective turnover time, which depends

on the depth of the convective layer, and is calculated theoretically as a function of spectral class (or, equivalently, colour index). Noyes et al. (1984) fitted the following empirical relation for Main Sequence stars:

$$\log \tau_{\mathrm{conv}}(x) = \begin{cases} 1.362 - 0.166x + 0.025x^2 - 5.323x^3, & x > 0 \\ 1.362 - 0.14x, & x < 0 \end{cases} \tag{2.2}$$

where $x = 1 - (B - V)$, with $B - V$ being the colour index.

Instead of the Rossby number, often the inverse Rossby number $Ro^{-1} = \tau_{\mathrm{conv}}/P_{\mathrm{rot}}$ is used, which correlates directly with magnetic activity. Sometimes, a coefficient of 4π is combined to it. This is also called the Coriolis number:

$$Co = 4\pi Ro^{-1}. \tag{2.3}$$

This definition is often used in dynamo theory.

The anticorrelation between the Rossby number and other indices describing stellar activity, such as the chromospherical index R'_{HK} (see section 2.4) was found by Noyes et al. (1984). This means that rapid rotators with deep convective layers tend to be the most magnetically active stars. The Sun is a considerably slow rotator, one rotation taking about a month. Using values from Noyes et al. (1984), the Rossby number for the Sun would be around 2, when it is around 0.1 for very active stars.

Rapid rotation also slightly decreases the luminosity of the star, because rotation adds to the outward oriented pressure forces, balancing against the inward gravitational force, thus also increasing the radius of the star. This decreases the density and temperature of the stellar core, where the energy production happens, thus decreasing the efficiency of the nuclear fusion (Faulkner et al., 1968).

2.2.1 Differential rotation

Since stars are not solid objects, their rotation is not necessarily uniform. Differential rotation is thus a common stellar phenomenon. In the Sun, this is easiest seen when studying sunspots at different latitudes: spots close to the equator rotate with a faster angular velocity than spots on higher latitudes. In addition to easily trackable sunspots,

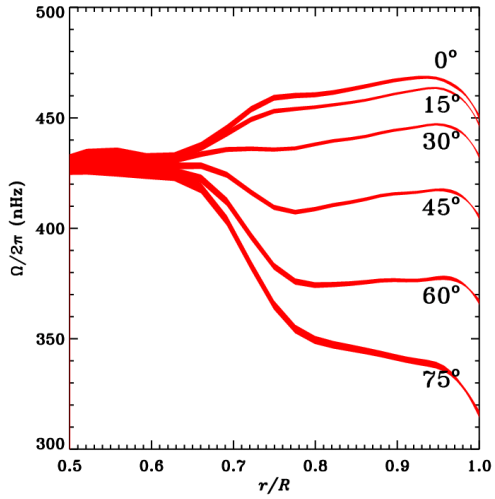

Figure 2.3: The internal angular velocity of the Sun, as a function of depth. The different lines correspond to different latitudes. Differential rotation can be seen above about 0.6 solar radii. Figure by the Global Oscillation Network Group (GONG) of the National Solar Observatory (NSO).

other surface structures are also used to measure the differential rotation; this is needed, since spots are concentrated on specific latitudes, rarely more than 30 degrees from the equator (see figure 2.6 and section 2.3.2). The rotational surface velocities can also be measured from Doppler shifts of spectral lines at the edge of the solar limb.

Furthermore, helioseismology has shown, that in addition to depending on the latitude, the rotational velocity also depends on the depth (figure 2.3). The radiative zone of the Sun is thought to rotate more or less uniformly. However, a recent study by Fossat et al. (2017) found the solar core to have a rotational period of about one week, which is approximately four times faster rotation than in the surface layers. The details of the internal solar rotation between the core and the outer zones still remain to be discovered. In the outer parts, differential rotation is seen in the convective zone, above the so called tachocline, which marks the transition region between the radiative and convective zones, at approximately 0.6 solar radii.

There are two commonly used indices to measure differential rotation. The amount of differential rotation relatively to the rotational velocity is calculated as:

$$\alpha = \frac{\Omega_{\mathrm{eq}} - \Omega_{\mathrm{pol}}}{\Omega_{\mathrm{eq}}}, \tag{2.4}$$

where Ω_{eq} is the angular velocity at the equator and Ω_{pol} at the poles. In the Sun, α yields values around 0.2 (Berdyugina, 2005, p. 33).

Some times differential rotation is expressed as the absolute difference between the equatorial and polar angular velocities, also called the rotational shear:

$$\Delta\Omega = \Omega_{\text{eq}} - \Omega_{\text{pol}}, \tag{2.5}$$

From $\Delta\Omega$ we can estimate how long it will take for the faster rotating equator to get a complete lap ahead of the poles. Using $\alpha = 0.2$ and $\Omega_{\text{eq}} = 0.25$ rad/d (Snodgrass and Ulrich, 1990) for the Sun, we get $\Delta\Omega_{\odot} \approx 0.05$ rad/d, and thus the equator would get one full lap ahead of the poles in ~126 days.

The differential rotation of the Sun approximately follows the empirical law:

$$\Omega(\phi) = \Omega_{\text{eq}} + \beta\sin^2\phi + \gamma\sin^4\phi, \tag{2.6}$$

where ϕ is the latitude, and β and γ are constants fitted to the observations. Often an approximation with $\gamma \approx 0$ is used. When solving β, for instance by inserting equation (2.6) for $\Omega_{\text{pol}} = \Omega(90^\circ)$ in equation (2.4), we get $\beta = -\alpha\Omega_{\text{eq}}$. This gives us the simple form:

$$\Omega(\phi) \approx \Omega_{\text{eq}}(1 - \alpha\sin^2\phi). \tag{2.7}$$

The coefficients commonly used for equation (2.6) are $\Omega_{\text{eq}} \approx 0.25$ rad/d, $\beta \approx -0.04$ rad/d and (if included) $\gamma \approx -0.03$ rad/d (Snodgrass and Ulrich, 1990).

2.3 Activity cycles

2.3.1 Solar activity reconstructions

The number of sunspots is the most commonly used proxy for solar activity. Historically it has been defined quantitatively by the Wolf Sunspot Number:

$$R = k(N + 10G), \tag{2.8}$$

where N is the number of individual sunspots seen on the Sun and G is the number of sunspot groups. The coefficient k is a normalization factor specific for each observer, depending on the instrumentation, observing conditions and the observer's eyesight, used to normalize the observations to the same level, originally that of Rudolf Wolf's own observations. This is generally done by daisy chaining, i.e. comparing the overlapping observational periods of different observers and adjusting k so, that their results for this period are as similar as possible. A plot of the Wolf sunspot series is shown in figure (2.4).

Since the physical basis for the Wolf Number is somewhat questionable as a profound indicator, suggestions for better formulations have been made. The Group Sunspot Number (GSN), introduced by Hoyt and Schatten (1998), ignores the number of individual sunspots and only counts the number of sunspot groups, or active regions. This is justifiable, as spots belonging to the same group are seen as part of the same magnetic disturbance. This also reduces observational errors, since groups are easier to separate than individual spots, which makes the old observations, done with poorer equipment, more reliable.

Also alternative versions for the Group Sunspot Number have been proposed, recalibrating the Hoyt and Schatten (1998) series. Hoyt and Schatten (1998) calibrated each observer similarly as Wolf originally did, by daisy chaining, i.e. calibrating new observers to the previous ones with overlapping data, leading to a chain of observers calibrated to each other. Another calibration method, the backbone method, was presented by Svalgaard and Schatten (2016). Here the chain of observers is reduced by choosing one 'backbone observer' for a certain time period as a reference observer, leaving some overlap in the time periods for different backbones, and each observer during that time period is then calibrated to the backbone observer. Then the periods with different backbone observers can be calibrated to each other using the overlapping observations.

The active day fraction (ADF) method, introduced by Usoskin et al. (2016), and updated by Willamo et al. (2017), completely avoids the problem of daisy chaining, which necessarily would lead to errors propagating through every new observer used in the chain. Instead, the ADF method compares the fraction of active days, when there are some sunspots reported, and spotless days, when there are no sunspots reported, by each ob-

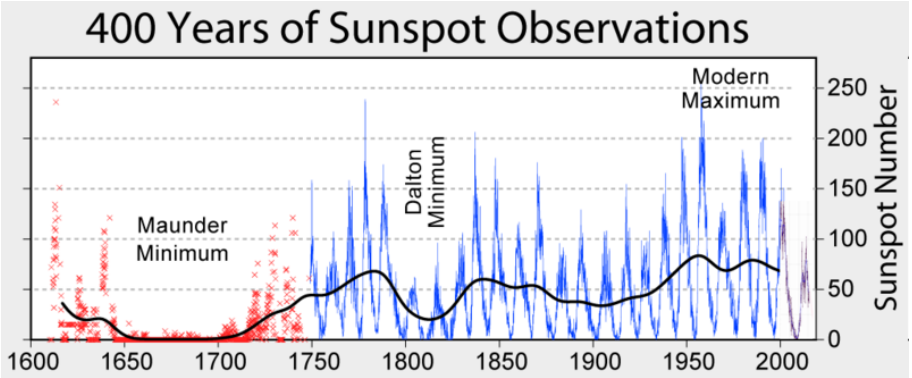

Figure 2.4: Monthly values of the Wolf Sunspot Numbers. Periods with enhanced or reduced activity are marked (the Modern Maximum, Maunder Minimum and Dalton Minimum). Image credit: Robert A. Rohde.

server to that of a reference data set of high quality. The active day fraction is an effective proxy for solar activity close to solar minima (Vaquero et al., 2015). The assumption is that, on average, the true ADF around solar minima remains the same for all observers, and the calibration is done by looking at how many spot groups the reference observer should have missed to gain a similar ADF as the observer. From this the calibration coefficients can be derived for each observer.

In addition to avoiding daisy chaining, another benefit of this method is that instead of giving each observer a single, constant coefficient k, it constructs a calibration matrix, where k is allowed to change as a function of the level of activity. The use of ADF statistics, however, assumes the Sun to be, on average, in a similar level of activity for all observers, so this method cannot be applied to periods of very low activity, such as the Maunder Minimum, when the reference observer, the Royal Greenwich Observatory, is set in the 20th century with moderately high activity. This calibration method also requires the observers to properly report spotless days, which is not always the case.

Figure (2.5) compares some of the different GSN reconstructions to each other. In the modern era the different reconstructions agree fairly well with each other, but in the earlier observations there are some differences. This is natural, since the quality of the data was not as good as with modern equipment, but it nevertheless presents some difficulties when trying to determine the exact level of solar activity through the centuries.

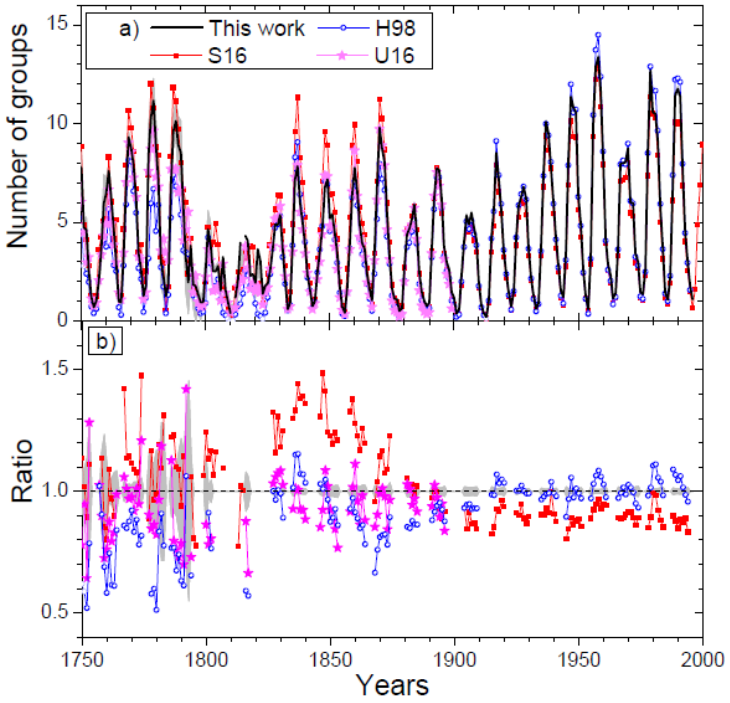

Figure 2.5: Comparison of the annual values of different reconstructions for the Group Sunspot Number series. Figure from Willamo et al. (2017). Upper panel: GSN-series from Willamo et al. (2017), Usoskin et al. (2016), Svalgaard and Schatten (2016) and Hoyt and Schatten (1998). Lower panel: Ratios between the other reconstructions and Willamo et al. (2017).

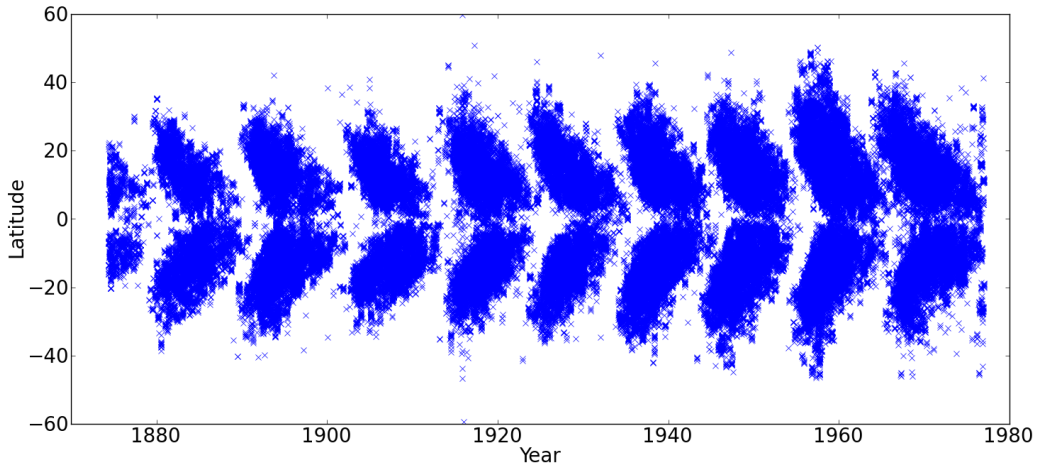

Figure 2.6: The famous butterfly diagram, showing the latitudes of sunspots as a function of time, plotted from sunspot data of the Royal Greenwich Observatory, available at http://solarscience.msfc.nasa.gov/greenwch.shtml.

2.3.2 The solar cycle

Solar cycles, each one lasting for approximately 11 years, are divided at solar minima to individual, numbered cycles, with the 1st cycle lasting from 1755 to 1766. Currently we are at the end of cycle 24, which started in 2008.

Observations of the latitude of the sunspots during the solar cycle have shown that in the beginning of the cycle, spots tend to form at higher latitudes, and as the cycle proceeds, they appear closer to the solar equator. During solar minima the number of spots is at its lowest. At the same time as the number of low latitude spots vanishes, spots start to appear again at higher latitudes, starting a new cycle. This pattern is known as the butterfly diagram (figure 2.6). This can be explained with a latitudinal dynamo wave shifting the magnetic field in the solar interior, but the precise mechanism still remains unclear. It is notable, however, that individual spots do not drift towards the equator, but rather follow the slow meridional flow towards the poles. It is rather the trend of where new spots on average are formed, which slowly moves to lower latitudes.

The cycle length is approximately 11 years, but varies a little each cycle. The phase of increasing activity is typically a few years shorter than the declining phase, as can be seen from figure (2.7).

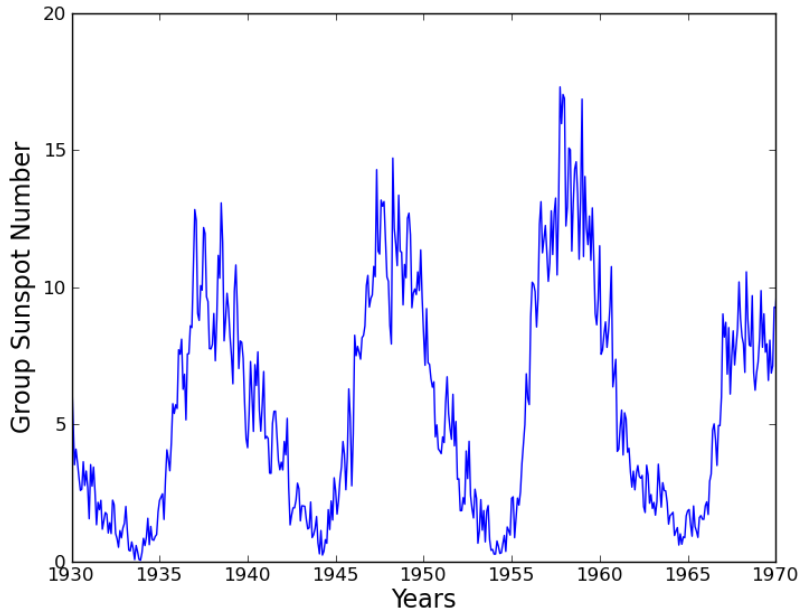

Figure 2.7: A more detailed view of the monthly GSN, produced from the data of Willamo et al. (2017). As can be seen, the phases of increasing activity are slightly shorter than the phases of decreasing activity during each cycle.

The strength of a solar cycle can be characterized by the amplitude of its maximum, or with the cycle intensity, which is calculated by summing all the sunspots or sunspot groups over a cycle, from minimum to minimum. A longer periodicity can be seen in these cycle strengths. This, approximately 80-year cycle, is known as the Gleissberg-cycle. In addition, the Sun has been exceptionally active during the 20th century, a period known as the Modern Maximum. There are also clear periods with reduced solar activity, most notably the Maunder Minimum, around 1650-1700, when almost no sunspots at all were reported (see figure 2.4). Another, lesser example is the Dalton Minimum in the beginning of the 19th century. More similar Grand Minima and Grand Maxima can be found in the extended series from the cosmogenic isotope reconstructions, which is shown in figure (2.8). Based on an analysis of the cosmogenic isotopes, Usoskin et al. (2007) concluded, that during the last 11000 years, the Sun has spent about 25% of its time in either a state of reduced or enhanced activity (Grand Minima or Grand Maxima).

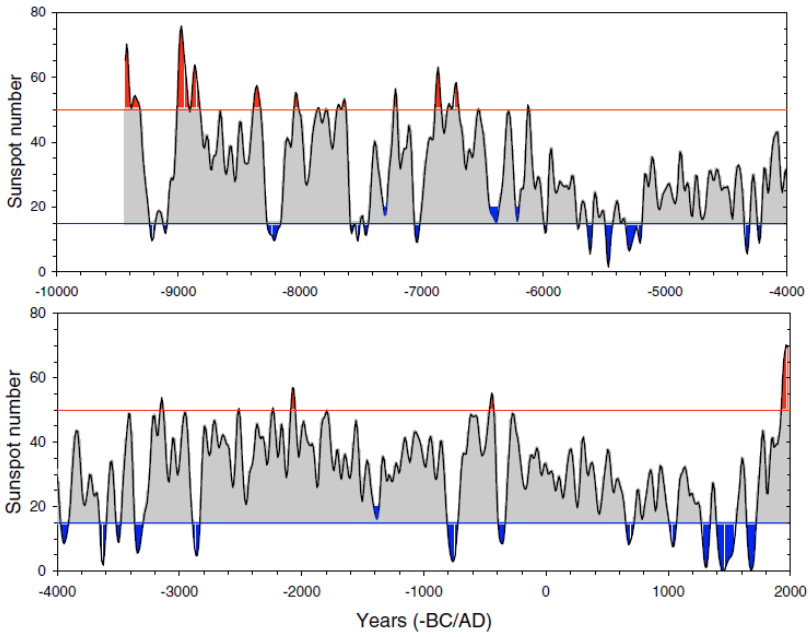

Figure 2.8: The sunspot number reconstructed through the Holoscene using cosmogenic isotopes. Red and blue areas represent Grand Maxima and Grand Minima, respectively. Figure from Usoskin et al. (2007).

2.3.3 Stellar cycles

Similar cycles to the 11 year sunspot cycle have been detected in other stars as well, varying in length from a few years to some 20 years (e.g. Lehtinen et al., 2016). However, in some cases very inconsistent cycle periods have been reported by different authors. For instance, with the star LQ Hya, period estimates vary from 2.5 years (Oláh et al., 2009, they reported three multiple periods ranging from 2.5 to 12.5 years) to 18 years (Lehtinen et al., 2016). Of course the cycle length can vary in reality, so some inconsistent results might be explained by that, but certainly there are still large uncertainties when defining stellar cycles.

Since no data sets as long as for the Sun are available, not that much can be said about activity in other stars on longer time scales than a few decades, although some variations can be seen in the scale of a few cycles. Furthermore, we cannot know, if a star, showing some activity, is in its normal state, or in a period of enhanced or surpressed activity, similar to the Maunder Minimum or Modern Maximum in the Sun. If the Sun can be used as an indicator here, these kind of activity changes are not uncommon.

Magnetic measurements have not been able to clearly prove the connection between starspots and magnetic fields. This might be because small scale magnetic fields with different polarities cancel each other out on larger scales, and the resolution which is achieved is not good enough to distinguish them, and only a larger scale magnetic field is seen. However, some hints of magnetic cycles have been found. In HD 29615, Hackman et al. (2016) found that the polarity of the global stellar magnetic field was reversed when compared to earlier observations made by Waite et al. (2015). The star seems thus to have undergone a polarity reversal, similar to that which the Sun goes through every new solar cycle.

The shape of stellar cycles is not purely sinusoidal. Reinhold et al. (2017) showed, that stellar cycles found from the Kepler photometric data tend to have a narrow peak at the maximum, whereas the minimum is more flatted. There does not, however, seem to be any significant difference in the duration of the phases of rising and decaying activity. The Kepler data allows, however, only discoveries of cycles significantly shorter than the solar cycle, because the space telescope has not been operating long enough. The longest cycles reported by Reinhold et al. (2017) are 6 years.

2.3.4 The Gnevyshev-Ohl rule

Looking at the solar cycle intensity, in most cases, though not always, the intensity of an odd cycle is higher than that of the previous even cycle. This was discovered by Gnevyshev and Ohl (1948) and is known as the Gnevyshev-Ohl rule. Some times the rule is presented in the form that odd cycles are generally stronger than even cycles, but in this form there exist more exceptions to the rule. In any case, the rule implies that it is physically justified to think of the cycles existing in pairs, which is also supported by the magnetic Hale cycle actually being twice as long as the 11 year Schwabe cycle.

A possible explanation for the Gnevyshev-Ohl rule could be a fossil field in the core of the Sun, oriented in such a way that it would add to the amplitude of certain polarity, making cycles with this polarity on average stronger than with reversed polarity (Ossendrijver, 2003, Chapter 5.1). However, such a field would slowly decay through magnetic diffusion, and it is difficult to understand how it could have persisted through

the entire lifetime of the Sun. Another possibile explanation to the Gnevyshev-Ohl rule is an extra dynamo mode.

According to Hale's polarity rule the polarity of the solar magnetic field is reversed between each cycle. However, there are observations of this only starting from the early 20th century; the polarity of the earlier cycles is deduced from the assumption, that it is reversed in each cycle. Callebaut et al. (2007) suggested that the polarity reversal would require a sufficiently strong cycle. Zolotova and Ponyavin (2015) built a thought experiment from this. If the 5th cycle during the Dalton minimum, lasting from about 1798 to 1810, would have been too weak to reverse the polarity, it would lead to a polarity reversal in all the previous cycles, compared to the classical view. This hypothesis would reconstruct the polarity in such a way, that the exceptions to the Gnevyshev-Ohl rule disappear, except for the last pair of two full cycles in the late 20th and early 21st century.

2.3.5 Stellar dynamo

In principle, the magnetic field of the Sun could be a fossil field originating from the interstellar cloud from which the Sun formed. This field should, however, have been lost through magnetic diffusion. This introduces the need for some mechanism generating the magnetic field, for which the dynamo theory is generally accepted. The stellar dynamo operates by converting mechanical energy (from rotation and convection) into magnetic energy.

There are two main effects contributing to the dynamo, which governs the stellar cycles, both changing the configuration of the magnetic field in different ways: the Ω and α -effects. In both of these, the key requirement is the 'frozen-in' condition of the magnetic field to the plasma. As long as this condition holds, two magnetically connected plasma cells will remain connected, which leads to the magnetic field following the movements of the plasma. In the outer parts of a stellar atmosphere this condition generally holds very well.

Differential rotation drives the Ω-effect. The field lines of a dipole field will get stretched and woven into each other due to the differential rotation. This transforms the initially poloidal (latitudal) field lines to toroidal (longitudal) ones.

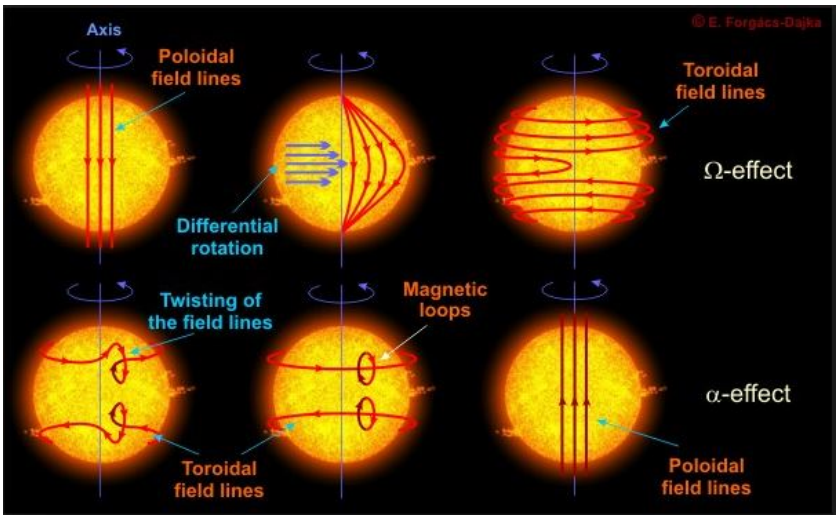

Figure 2.9: The α and Ω effects change the solar magnetic field in the course of one solar cycle. In the upper figures, the Ω-effect turns the poloidal field to a toroidal one. In the lower figures, the α-effect turns the field back to a poloidal one. Image credit: E. Forgacs-Dajka.

Turbulent convection drives the α-effect. As plasma rises from the stellar interiors, it carries magnetic field with it, and will thus radially disrupt horizontal magnetic field lines. This is also the key effect responsible for the generation of sunspots, since it drives the formation of radial magnetic loops, around which sunspots can form.

In the Sun both these effects play a part. At solar minimum the magnetic field is close to a poloidal dipole field, which then gets stretched by the Ω-effect. As the field lines end up closer and closer to each other, the magnetic activity increases, until solar maximum is reached, when the poloidal field has been stretched to a mostly toroidal field. When the field lines are chaotically woven into each other, they frequently form loops where sunspots can emerge (as seen in figure 2.1). Finally, the frozen-in condition temporally breaks down, allowing magnetic reconnection to happen due to the α-effect, and the field returns to its original poloidal configuration, with the polarity reversed. This is called an $\alpha\Omega$ -dynamo. The main stages of this dynamo are illustrated in figure (2.9).

The Hale rule for sunspot pairs can be explained by the Ω-effect. As differential rotation drags the magnetic field, the higher latitude parts of a field line are lagging behind the equatorial field. Thus, the spot closer to the equator will be leading the one at a higher latitude. Because no major reconnections have yet happened in the field lines,

the field at every latitude still points in the same direction as the initial poloidal field. This leads to the polarity between the spots being different on the two hemispheres, i.e. if the magnetic field on one hemisphere points from the leading to the trailing spot, it will point from the trailing to the leading one on the other hemisphere.

In more active stars the rotation tends to be faster, which makes differential rotation less efficient compared to the α-effect. This leads to the α-effect dominating the dynamo, which is called an $\alpha^2\Omega$-dynamo. Theoretical models show that the dynamo can sustain itself even without any differential rotation, (e.g. Rüdiger et al., 2001), in which case the α-effect is responsible for both the transformation from toroidal field to poloidal, as well as from poloidal to toroidal. This is called an α^2-dynamo. These kinds of dynamos are probably sustaining the magnetic fields in very active stars (e.g. Ossendrijver, 2003), although it is difficult to get observational evidence of the stellar dynamo mechanisms.

2.3.6 Active longitudes and flip-flops

In many stars active regions have been observed to concentrate on certain, active longitudes. Active longitudes have been observed in the Sun as well, but the question whether these are enduring phenomena is still not fully answered. Differential rotation complicates the search for active longitudes, since it is difficult to say when multiple spots on different latitudes arise from the same longitude, due to their different rotational velocities. Berdyugina and Usoskin (2003) analysed 120 years of sunspot data and came to the conclusion that two active longitudes persisted through this interval. However, Pelt et al. (2005) argued, that the results by Berdyugina and Usoskin (2003) could also be obtained from randomly distributed data. The question of solar active longitudes is thus still debatable. In rapidly rotating stars differential rotation is often not that strong, so active longitudes are easier to find.

When analysing photometry of FK Comae, Jetsu et al. (1993) found that the phase of the photometric minimum was shifted twice with half a period in their data. This was interpreted as two active longitudes, separeted by some 180 degrees, and apparently the spot activity was changing between these two. This phenomenon was labeled flip-flops. Korhonen et al. (2001) confirmed the change in dominating longitudes by spectroscopic

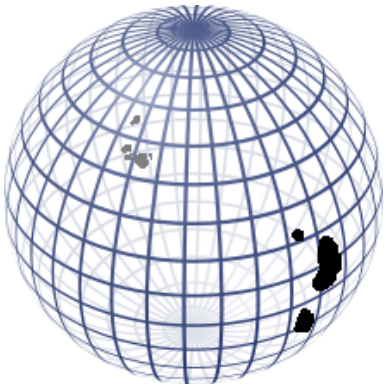

Figure 2.10: An illustration of two active longitudes (the regions with dark spots) on the opposite sides of a spherical star. In the case of flip-flops, the spot activity would shift between these regions.

Doppler imaging of FK Comae. Berdyugina and Usoskin (2003) also reported flip-flops in the sunspot data, but the reliability of this was again questioned by Pelt et al. (2005).

Figure (2.10) illustrates two active longitudes, separated by about 180 degrees, on the surface of a spherical star.

2.4 Other indicators of magnetic activity

In addition to the phenomena described above, there also exist several other indicators of stellar magnetic activity. These are not considered in the data analysis, which is focused on the phenomena observable from Doppler imaging and photometric time series analysis, but should be mentioned, nevertheless. One is chromospheric activity. The chromosphere is the layer of the stellar atmosphere above the photosphere, characterised by emission lines, in contrast to the absorption lines of the photosphere. The density drops rapidly in the chromosphere, but the temperature rises several thousand degrees above that of the photosphere.

Chromospheric activity is seen in all active stars, as well as in the Sun. It is maintained by convection in the layers below. The most common signs of chromospheric activity are the Ca II H&K emission lines, whose intensity vary periodically in correspondence to the stellar cycle, as was first suggested by Wilson (1978).

A common index used to describe chromospheric activity is R'_{HK}, or its logarithm, which gives the amount of the total luminosity of the star radiated in the two chromo-

spheric calcium lines (H and K):

$$R'_{\rm HK} = \frac{L_{\rm HK}}{L_{\rm bol}}, \tag{2.9}$$

where $L_{\rm bol}$ is the star's bolometric luminosity.

The solar mean value for this index is $\log R'_{\rm HK} = -4.614$ (Noyes et al., 1984), a fairly intermediate value for solar-type stars. Other emission lines, whose intensity is used as a proxy for chromospheric activity, include Hα and Mg II (e.g. Hall, 2008).

The outermost layer of the solar atmosphere is called the corona. This consists of extremely thin and hot gas. The complete heating mechanisms of both the chromosphere and the corona are still debated (e.g. Aschwanden et al., 2001). Energetic eruptions through the corona are quite common, such as flares and Coronal Mass Ejections (CME). They occur when energy stored in the magnetic field is released through magnetic reconnection.

Flares are intensive flashes of high energetic radiation, originating from plasma falling down through the chromosphere in reconnection of magnetic field lines above active regions. Flares are rapid events, occuring on the scale of minutes to hours. In a Coronal Mass Ejection magnetic reconnection allows the plasma to escape the magnetic field, and large amounts of high energetic cosmic particles are released. These two events are often, but not always, connected to each other. Stellar flares are easily observed, since they cause the star to brighten considerably. CMEs from other stars are more difficult to observe, because, unlike in flares, the main part of the energy is released as high energetic particles, whose trajectories are affected by magnetic fields. As a consequence, the origin of these cosmic rays is extremely difficult to deduce. Still, they can be deteced for instance by the blueshift an ejection directed towards the observer causes on the spectral lines, when the erupting material is moving with high speed away from the stellar surface (e.g. Vida et al., 2016). Solar CMEs can even have an effect on society, as they may disturb satellites and even electrical devices on the surface of the Earth.

2.5 BY Draconis -stars

BY Draconis -stars, to which the object of this study, V889 Her, belongs, are late type variables, with spectral classes varying from G to M, characterized by low amplitude brightness variations of up to about 0.5 magnitudes (usually much less) due to inhomogeneities (dark spots and bright faculae) in the photosphere, and by changes in chromospheric emission. When the star rotates, different parts of the surface are seen to the observer, leading to periodic variations in the magnitude, with the period corresponding to the rotation of the star. BY Dra -stars are closely related to flare stars of UV Ceti -type. In both classes the variability is caused by magnetic activity, but in flare stars the strong flare eruptions lead to considerably greater amplitudes in the photometric variations, often lacking clear periodicity.

Observationally, Bopp and Fekel (1977) defined the BY Draconis class to include stars fulfilling the following criteria: they must (1): show low-amplitude variability with a period of a few days, (2): be of spectral type K or M, and (3): their spectrum must contain emission lines of Ca II (and often also Hydrogen). In practise, however, also many G-type stars are classified as belonging to the BY Draconis class.

Physically, BY Dra -stars are young, solar-like stars, with strong magnetic fields and rapid rotation. Probably the Sun has resembled these kind of stars in its youth. In contrast to the present Sun, large spots dominate the luminosity variations, which leads to luminosity maximum corresponding to activity minimum, and vice versa (Radick et al., 1990).

The archetype of the class, BY Draconis, was originally thought to be a UV Ceti -type star due to detections of strong chromospheric emission in Hydrogen Balmer lines and Calcium II H&K lines (Popper, 1953). However, no flares were detected, and Chugainov (1966) proposed spots to be the cause of the photometric variations. Earlier, Kron (1952) had suggested inhomogeneities on the surface to be the reason for photometric variations on YY Gem, another star, which later was categorized as a BY Dra -type of variable.

Because BY Dra -stars are generally rapid rotators, differential rotation should not be very effective. Thus, in contrast to the Sun, their magnetic activity is probably sus-

tained by either an $\alpha^2\Omega$ or α^2 -type dynamo.

2.6 Evolution of solar-like stars

Stars are formed as fragments of clouds of interstellar gas, collapsing due to gravity. At first the protostar gets its energy from gravitational contraction. Because the angular momentum of the initial cloud is conserved, the rotation of the star increases as its radius decreases. Observations confirm that young stars are rapid rotators.

The angular momentum of the initial, collapsing cloud fragment most likely originates from turbulence in the interstellar medium (Fleck and Clark, 1981). Because of the random nature of turbulent forces, the rotational axes of stars end up being randomly oriented, which agrees with observations (Bouvier, 1991), in contrast of the earlier hypothesis that the rotation originates from galactic differential rotation, which would lead to differences in rotational properties depending of the birth place of the young star. This is not seen, but young stars in different clusters seem to have similar rotational properties, independently of their galactic location (Bouvier, 1991).

In this early evolutionary phase the young solar-type star is still mainly fueled by gravitational contraction, and often surrounded by a dust shell, where possible planet formation might be going on. The surface temperature is already close to that of a Main Sequence star of similar mass. This is called the T Tauri phase, which lasts for some 10 million years.

Finally, when the temperature and density in the center of the contracting protostar get high enough, nuclear fusion starts burning hydrogen to helium, and the star moves to the Main Sequence. Due to the stellar winds carrying away angular momentum, the rotation slows down as the star ages, and the magnetic activity decreases, as suggested by the Rossby number (equation 2.1). In a recent study by Rosén et al. (2016), a significant decrease of magnetic activity was found between ages 50-250 million years, whereas there was no significant changes between 250-600 million years. However, their sample of stars was quite small to draw any definite conclusions from.

In young solar-type stars, luminosity variations are generally dominated by dark

spots, whereas bright faculae overcome the darkening effect of spots in older stars, such as the Sun, although the variations in these are generally much weaker. In solar mass stars this change from spot-dominated luminosity variations to faculae-dominated variations is estimated to happen around the age of 1 billion years (Radick et al., 1990).

Solar analogues are single stars with similar mass and chemical composition as the Sun. After the T Tauri -phase, they typically become BY Dra -variables. The BY Dra -phase lasts considerably longer than the T Tauri -phase, but eventually the stellar wind will carry away enough angular momentum to decrease the magnetic activity, as has happened in the Sun, which is not anymore a particularly active star. An exception to this are the RS CVn -binaries, whose magnetic activity can last to a consiberably older age because the close binary system is able to sustain the rapid rotation due to tidal locking of the rotational periods.

A solar mass star stays in the Main Sequence for roughly 10 billion years, the Sun being about half way through its lifetime. During this core hydrogen burning phase, the star stays sufficiently constant. During the evolution from a BY Dra -variable to a star resembling the Sun today, rotation and magnetic activity decrease. The luminosity, on the other hand, slowly increases, as more and more hydrogen is fused to helium. Theoretically the relation between luminosity, mass and chemical composition of a solar mass Main Sequence star, where the opacity follows Kramers' opacity law ($\kappa \propto T^{-3.5}$), should be:

$$L \propto m^{5.5}\mu^{7.5}, \tag{2.10}$$

where m is mass an μ the mean atomic weight (Clayton, 1983, p. 470). The observed relation for the luminosity and mass is, however, closer to $L \propto M^4$, although quite varying exponents have been used, e.g. $L \propto M^{4.5}$ in Salaris and Cassisi (2005, p. 139), $L \propto M^{4.0}$ in Duric (2004, p. 20), and $L \propto M^{3.8}$ in Karttunen et al. (2010, p. 320).

Whatever the precise form of the relation, the key point is that luminosity depends very strongly on both mass and the mean atomic weight. As hydrogen is fused to helium, μ increases, and so does the luminosity. The mass can be assumed to stay constant, because the amount of mass loss due to nuclear fusion and stellar winds is negliglible at this evolutionary stage. Because the luminosity slowly increases during the Main Sequence

evolution, the Sun is somewhat brighter now than it was during its youth.

3. Methods

This chapter will describe the methods used for analysing the data of V889 Her. These include spectroscopic Doppler imaging, a powerful tool to resolve details on stellar surfaces, and a photometric time series analysis method called Continuous Period Search. Also the power spectrum -method, which is used to search for the best period for the activity cycle, is presented briefly.

3.1 Doppler imaging

As almost all stars appear as point sources even to the most advanced telescopes, usually no features from their surface can be directly resolved. The Doppler imaging method makes it possible to indirectly map the surface of a rotating star through asymmetries arising in the spectral lines, caused by inhomogeneities in the temperature on a rotating star's surface.

A colder spot on the star's surface emits less radiation than a hotter area. Depending on the location of the spot, the light we observe may be blueshifted or redshifted due to the star's rotation, as the spot is either moving towards or away from the obserever. The lower temperature of a spot decreases the continuum level at the parts of an absorption line affected by the spot. Even if the spot woud cause a stronger absorption line, the amount of absorbed flux will be less because of the reduced continuum. Thus, the net effect of a spot will be a 'bump' in the spectral line profile, with the location of the bump corresponding to the location of the spot in radial velocity space (see figure 3.1). As the star rotates, the radial velocity of the spot will change. This is seen as a movement of the bump across the line profile.

Deutsch (1958) was the first to consider resolving details of stellar surfaces through Doppler broadening of spectral lines. Goncharskii et al. (1977) developed the method further, and resolved chemical inhomogeneities with it. Vogt and Penrod (1983), Vogt et al. (1987) and Piskunov et al. (1990) developed the technique to be applied to cool spots. In magnetically active stars the surface layers are convective, which leads to mixing of different elements. Thus, in these stars there are no significant chemical inhomogeneities, and the main factor affecting spectral line profiles is temperature.

In order for the Doppler imaging method to be applicable on a star, the star needs to rotate rapidly enough for the spectral lines to be wide enough to be resolved properly. Rotational Doppler broadening has to dominate over other forms of line broadening (e.g. thermal motion, convective turbulence, oscillations) in order for reliable results. The star is also required to be quite bright, so that good enough spectra can be gained. This requires sufficiently large telescopes and good instruments to achieve high resolution spectra, because the exposure times cannot be too long, as that would lead to changes in the rotational phase of a fast rotator during the exposure. Several spectra are needed of different rotational phases, in order to cover the whole surface of the star.

In practise, what we want to do, is to find a temperature distribution for the stellar surface, which, with a given rotation, would minimize the difference between the model and the actual data. For this we construct an error function D:

$$D = \sum_{\phi,\lambda} \omega_\phi(\lambda) \frac{(r_{\phi,\mathrm{mod}}(\lambda) - r_{\phi,\mathrm{obs}}(\lambda))^2}{N_\phi N_\lambda}, \tag{3.1}$$

where r is the value of the data point in the spectrum, subscripts *mod* and *obs* corresponding to the model and the observation, respectively. ω is the weight of the data point, inversely proportional to the square of its observational error, ϕ the rotational phase, N_ϕ the number of rotational phases used, and N_λ the number of wavelength points in each spectrum. The difference is summed over every wavelength, and over all phases observed.

The model surface of the star is divided into a grid of latitudes and longitudes. Each of these elements has a certain temperature, which will affect the line absorption properties of the stellar atmosphere. These are calculated from atmospheric models for

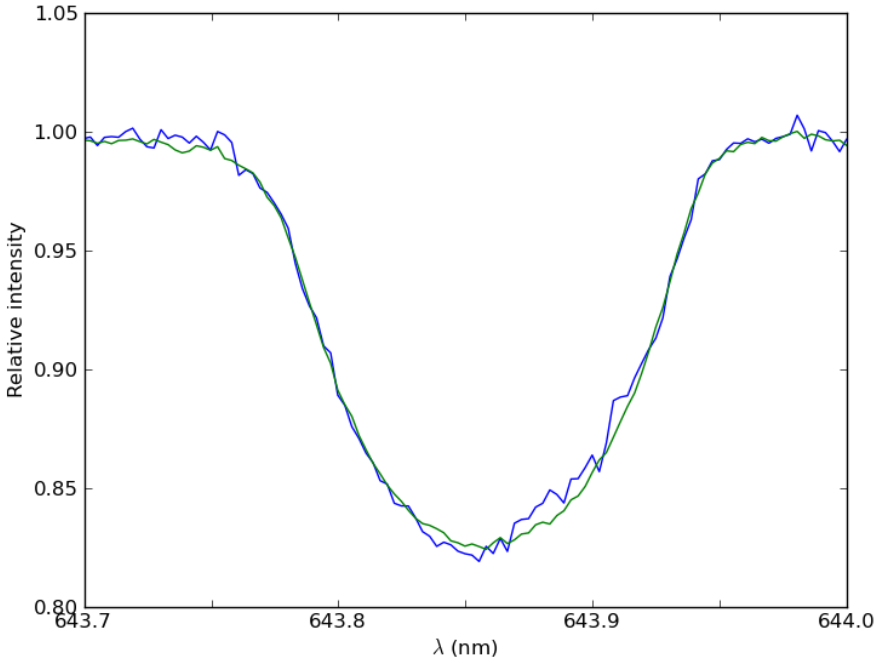

Figure 3.1: The line profile of a Ca I absorption line in V889 Her. The blue curve shows the line in an individual spectrum, the green is a mean line profile of 17 spectra from different rotational phases. The green line should thus represent the line when it is relatively unaffected by cool spots. In the blue line some effects of spots can be seen as deviations from the mean line profile, mainly the bump on the right side of the centre, corresponding to a cool spot which is redshifted, i.e. rotating away from the observer.

different temperatures and limb angles, with a given chemical composition. The value of the intensity for a certain wavelength point is summed together over each grid point in equation (3.1). The temperature distribution which minimizes the error function D gives the desired temperature map of the stellar surface.

Suitable lines for Doppler imaging are intermediately strong photospheric absorption lines. Most commonly neutral metal lines, such as Fe I and Ca I, in the wavelength region around 500-800 nm, are used. A number of different absorption lines can be combined to increase the accuracy of the map.

Crucial parameters in the Doppler imaging program include the inclination i, the rotational velocity projected on the line of sight $v \sin i$, where v is the rotational velocity and i the inclination, the rotational period P_{rot}, and the differential rotation parameter α (equation 2.4). Other parameters, with physically less trivial interpretations, are microturbulence v_{mic} and macroturbulence v_{mac}, which describe velocity dispersion due to turbulent effects. They are distinguished by the size of the turbulent element: if the size is small compared to unit optical depth, the turbulence is called microturbulence, and if the size is large when compared to the unit optical depth, the turbulence is called macroturbulence (Gray, 2005, p. 423). Macroturbulence is mainly caused by convection, whereas microturbulence is caused by smaller scale effects, whose origin is not yet completely understood. Both these have a broadening effect on line profiles. However, microturbulence might strengthen the line, whereas macroturbulence just broadens it (Gray, 2005, chapter 17).

An extension of Doppler imaging is Zeeman-Doppler imaging (ZDI), which was introduced by Semel (1989). ZDI allows one to map the distribution of magnetic field on the stellar surface, by measuring polarization in the line profiles, caused by the Zeeman effect in the presence of a magnetic field. Usually only circular polarization (Stokes V parameter) is used, because it is much stronger in active stars than linear polarization (Stokes Q and U parameters). However, if linear polarization is also taken into account, using all four Stokes parameters (Stokes I, characterising the unpolarized brightness, being the fourth parameter), the magnetic field structure can be derived more accurately (Rosén et al., 2015). By using both Doppler imaging and Zeeman-Doppler imaging, cor-

relations between cool spots and strong magnetic fields have been searched for, although this relation has been weaker than expected, as mentioned in section (2.3.3). Although a powerful tool, ZDI is not used in this thesis, because it demands spectropolarimetry. Only spectroscopic data has been used here.

There has been some discussion about the reliability of Doppler imaging, particularly regarding the polar spots observed in some stars, and whether chromospheric activity could cause similar line profiles (e.g. Unruh and Collier Cameron, 1997; Bruls et al., 1998; Strassmeier et al., 1993). Strassmeier et al. (1993) speculated if a chromospheric velocity field, bright plages moving across the stellar disk, or unresolved circumstellar absorption could cause similar line profiles. Byrne (1996) suggested that incomplete understanding of the atmosphere producing the spectral lines could be the reason for this. This is to say, that if we don't fully understand the production of unspotted spectral lines, how can we then understand the effect spots cause? However, interferometric observations have been able to directly confirm the existence of polar spots in the RS CVn type star ζ And (Roettenbacher et al., 2016), producing real images with darker polar areas, so the polar spots produced with Doppler imaging can be regarded with at least some certainty. Also Bruls et al. (1998) reach the conclusion that, even if chromospheric activity may play a part, it cannot be responsible for all the effects seen in the line profiles of active stars, which supports the existence of polar spots.

3.2 Photometric time series analysis

Sufficiently long time series, covering decades of photometric data, are available for many active stars. Periods and amplitudes of the brightness variations of the star can be derived from these. This can reveal a periodicity due to the rotation of the star, but also, if there are observations for a long enough time, activity cycles corresponding to the solar 11 year cycle. Active longitudes and flip-flops can be found by studying the phases of the light curve minima, which correspond to the dominating spot facing the observer; when the spot rotates out of view, the star brightens.

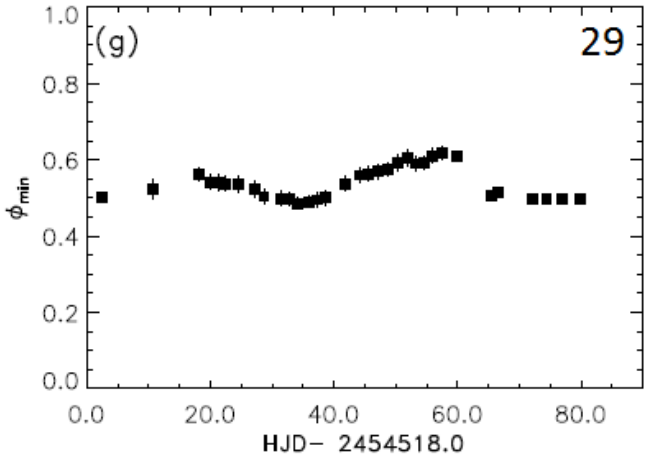

Figure 3.2: An example of what a short termed active longitude looks like in segment 29 of the data of V889 Her. The black boxes show the phase ϕ of each photometric minimum. All minima are concentrated at the same phase, $\phi \approx 0.5$.

The rotational phase ϕ is defined as

$$\phi(t) = FRAC(\frac{t - t_0}{P}), \tag{3.2}$$

where t is the time of the measurement, t_0 is a constant reference time, P is the rotational period, and the function $FRAC$ removes the integer part of the numerical value.

Here again, differential rotation complicates the derivation of rotational periods, since spots on different latitudes cause periods of different length.

Figure (3.2) shows an example where the photometric minimum occurs on a constant phase, which could be interpreted as a single spot/spot group dominating the light curve, staying always on the same longitude (at least for the time span of the data set). If this behaviour continues for long enough, the longitude is defined as 'active'.

Generally the best period is searched by fitting sinusoidal functions of some chosen form to the data. The period is a free parameter in the fit, and the period which minimizes the errors between model and observations is searched. For instance, Three Stage Period Analysis (TSPA), formulated by Jetsu and Pelt (1999), uses the following series:

$$g(f) = M + \sum_{k=1}^{K} [B_k(f)\cos(k2\pi ft) + C_k(f)\sin(k2\pi ft)], \tag{3.3}$$

where M is the mean magnitude, and the best frequency $f = 1/P$, with P being the period, is fitted, along with the coefficients B_k and C_k, for each k. K is the order of the model, with a higher value taking into account higher order terms. With a higher K the fit gets better, but if it is too high, the model starts overfitting, treating random noise as real features. Often more than a single sinusoid is required, because the spot configuration can be complex. There can be multiple spots causing multiple minima to the light curves, with the amplitude corresponding to the projected size of the spot.

3.2.1 The Continuous Period Search -method

The Continuous Period Search -method (CPS), which is used in this thesis, was developed from the Three Stage Period Analysis, and was formulated by Lehtinen et al. (2011). The data is fitted with a similar model as equation (3.3). The main improvements from TSPA are a better time resolution, achieved by allowing the time frame to move as a sliding window, which also allows one to continuously study changes in the period, and other parameters. This is a great advantage, because the changes in real stars can happen on short time scales. Changing periodicity can be interpreted as differential rotation, as spots with different rotational velocities would have rotational periods of varying length. The amount of differential rotation can be estimated from the dispersion of the best fit values for the period. Another possibility causing changes in the period, however, might be changes in the spot configuration. If the dominating spot or active region moves longitudinally, with respect to the rotation, it will lead to a different apparent photometric period than the true rotational period.

CPS works by dividing the data into smaller sets, which are analysed individually. The length of these data sets is chosen so that there is enough data to do accurate modelling, but the set is not so long that the light curve would have time to change significantly. Lehtinen et al. (2011) states that in practice, suitable lengths for the data sets are between 25 and 200 days, when analysing ground-based photometry of active stars.

Each data set with at least 10 data points is considered to have enough data to be modeled. The sets are allowed to overlap, which enables the flexibility of continuously following changes in the parameters. A new set is started either at each new data point, or

each new observing night. When choosing the time frame for the next set to be analysed, it is always required that the next set must have at least one data point which did not belong to the previous set. The best period, mean magnitude, amplitude, and phase of the minimum is found for every set. Since there are overlapping data points, it is notable that all estimates are not independent of each other.

The data is further divided into separate, longer segments, whenever there are long gaps in the observations. This allows to separate different observational seasons from each other, which is convenient when analysing photometric data such as that in this thesis, because there are long, periodic gaps in the data due to seasonal variations in the observing conditions.

The order of the model (K in equation 3.3), in other words the number of sinusoidal curves fitted to the data, is derived using the Bayesian information criterion, as presented by Stoica and Selén (2004):

$$R_{\mathrm{BIC}} = 2n \ln \left(\sum_{i=1}^{n} [\sigma_i^{-2} \epsilon_i^2] [\sum_{i=1}^{n} \sigma_i^{-2}]^{-1} \right) + (5K + 1) \ln n. \tag{3.4}$$

Here σ_i is the observational error of the data point, ϵ_i is the residual, i.e. the difference between the model and the observed data point, and n is the number of data points. The first term is reduced by higher orders taken into account, which allows for a better fit. The second term is a penalty term, used to avoid overfitting, which grows larger for a higher order. The value of K which minimizes R_{BIC} is defined as the optimal order. K is, however, not allowed to exceed the limiting order K_{lim}, so values between $0 \leq K \leq K_{\mathrm{lim}}$ are tested. For spotted stars, a limiting order $K_{\mathrm{lim}} = 2$ is commonly used.

Data sets are further divided into reliable and unreliable ones. Here the reliability is determined by a Kolmogorov-Smirnov test, as was done in TSPA (Jetsu and Pelt, 1999). A random bootstrap sample with a sample size $S = 200$ is drawn for each parameter. For each random value x_i of a parameter, the value is transformed to a variable $u_i = (x_i - m_x)/s_x$, where m_x is the mean, and s_x the standard deviation of the random bootstrap set of parameter vaules. The Kolmogorov-Smirnov test is used to determine, whether this bootstrap distribution is drawn randomly from a Gaussian distribution. For these samples

the Kolmogorov-Smirnov test statistic a is calculated as:

$$a = \max(|F_s(u) - F(u)|), \tag{3.5}$$

where the max-function gives the maximal value of its argument. Here $F_s(u)$ is the cumulative distribution function, defined as

$$F_s(u) = \begin{cases} 0, & u < u_1 \\ i/S, & u_i \leq u < u_{i+1} \\ 1 & u > u_S, \end{cases} \tag{3.6}$$

and $F(u)$ is the cumulative Gaussian distribution function:

$$F(u) = (2\pi)^{-1/2} \int_{-\infty}^{u} e^{-z^2/2} dz. \tag{3.7}$$

The test statistic a is the maximum value for the absolute difference between these, from the randomly drawn bootstrap sample. The set is considered unreliable if

$$a \geq c(\alpha = 0.01), \tag{3.8}$$

where α is the desired significance level, and c is the upper limit for a, if the sample is indeed drawn from a Gaussian distribution. A conservative significance level of $\alpha = 0.01$ can be used, leading to sufficiently reliable results, because there is fairly large amounts of data available. In a Kolmogorov-Smirnov test, the limit $c(\alpha)$ is calculated as

$$c(\alpha) = \sqrt{-\frac{1}{2} \ln(\frac{\alpha}{2})}, \tag{3.9}$$

and for the desired significance level, the value is $c(\alpha = 0.01) \approx 1.63$,

A secondary minimum is furthermore considered unreliable if it is not included in at least 95% of the bootstrap samples (=190, when the sample size is $S = 200$).

If any of the parameters (with the exception of the phase of a secondary minimum) fails the test, every parameter in that set is considered unreliable.

3.2.2 Power spectrum

The length of a longer activity cycle can be determined by time series analysis of the mean magnitudes for each set, derived from the CPS analysis. Here the power spectrum method has been used, as presented by Scargle (1982). The power spectrum index z for a frequency f is:

$$z(f) = \frac{[\sum_{i=1}^{n}(y_i - \hat{y})\cos(2\pi f(t_i - \tau))]^2}{2\sum_{i=1}^{n}\cos^2(2\pi f(t_i - \tau))} + \frac{[\sum_{i=1}^{n}(y_i - \hat{y})\sin(2\pi f(t_i - \tau))]^2}{2\sum_{i=1}^{n}\sin^2(2\pi f(t_i - \tau))}. \tag{3.10}$$

Here y_i and t_i are the i:th data point (magnitude) and time point, and $\hat{y}$ is the mean magnitude. τ is defined as

$$\tau = \frac{\arctan\left(\frac{\sum_{i=1}^{n}\sin(4\pi f t_i)}{\sum_{i=1}^{n}\cos(4\pi f t_i)}\right)}{4\pi f}. \tag{3.11}$$

The frequency which maximizes z gives the best period for the activity cycle as $P_{\mathrm{cyc}} = 1/f$.

4. V889 Herculis

The object of this study, V889 Herculis (HD 171488), is a young solar analogue; a single, magnetically active star of spectral class G2 V (Montes et al., 2001; Henry et al., 1995), classified as a BY Draconis -variable (Kazarovets and Samus, 1997), with a mass only slightly higher than the Sun's. Strassmeier et al. (2003) were the first to closely study the star. They found a rotational period $P_{\mathrm{rot}} = 1.3371$ d, making it a very rapidly rotating star (compare to the Sun, for which one rotation takes about a month). They also produced the first Doppler image of the star, and found a large polar spot, which has been confirmed in later studies, (e.g. Marsden et al., 2006; Järvinen et al., 2008; Frasca et al., 2010).

V889 Her is still a very young star, as can be expected from its fast rotation. Its age has been estimated to be around 30-50 million years (Strassmeier et al., 2003; Frasca et al., 2010). The star has a very similar surface temperature to the Sun (both belong to the spectral class G2 V). Although the Sun is much older, and has moved higher on the Main Sequence during its billions of years of evolution, V889 Her has a slightly higher mass, so it belongs to a slightly earlier spectral class than the Sun presumably did at a similar age.

One controversial aspect of V889 Her is its differential rotation. Marsden et al. (2006) and Jeffers and Donati (2008) measured a very high differential rotation, by fitting similar curves as for the solar differential rotation (equation 2.6, with $\gamma = 0$). For the rotational shear (equation 2.5), Marsden et al. (2006) gained the value $\Delta\Omega = 0.402 \pm 0.044$ rad/d, and Jeffers and Donati (2008) $\Delta\Omega = 0.52 \pm 0.04$ rad/d or $\Delta\Omega = 0.47 \pm 0.04$ rad/d, using both brightness data (Stokes I parameter) and magnetic data (Stokes V parameter), respectively. These values would make V889 Her one of the most differentially rotating

known stars. This would be somewhat unexpected for such a rapid rotator, because differential rotation is not expected to increase with increasing rotational rate (Reiners and Schmitt, 2003). However, Huber et al. (2009) found no differential rotation at all, although their analysis does not strictly exclude it either. Kővári et al. (2011) found $\Delta\Omega = 0.042$ rad/d, which is close to the solar value ($\Delta\Omega_\odot \approx 0.05$ rad/d). Thus, the question of differential rotation still remains somewhat unclear. As can be seen from the inconcistent results, this is a quantity which is very difficult to measure using Doppler imaging.

It is worth noting, that even though according to this definition for differential rotation (equation 2.5), the values by Marsden et al. (2006) and Jeffers and Donati (2008) are larger than the solar value, the relative differential rotation (equation 2.4) without error bars is only $\alpha \approx 0.084$ for Marsden et al. (2006) and $\alpha \approx 0.105$ or $\alpha \approx 0.097$ for Jeffers and Donati (2008), while the solar value is around $\alpha \approx 0.2$. This means that the differential rotation would still not be very large when compared to the rotation of the star, although the rapid rotation would make the absolute value of the differential rotation very large.

Lehtinen et al. (2016) found a photometric rotational period of 1.3454 days, as well as a longer, 9.5 year activity cycle for V889 Her, with an increasing mean magnitude. They also found the chromospheric emission index $\log(R'_{\mathrm{HK}}) = -4.175$, making V889 Her chromospherically a very active star (Lehtinen et al. (2016) defined very active stars to have $\log(R'_{\mathrm{HK}}) > -4.20$). They give the value $\log(Co) = 1.98$ for the Coriolis number of V889 Her, which is related to the Rossby number as $Co = \frac{4\pi}{Ro}$, corresponding to $Ro \approx 0.13$. Henry et al. (1995) give the value $Ro \approx 0.06$.

From equation (2.2), by using the approximate value $B - V = 0.62$ for V889 Her (see figure 5.11 and the end of section 5.2.2), we would get $\tau_{\mathrm{conv}} \approx 10.2$ d, and by using $P_{\mathrm{rot}} \approx 1.3$ d, the Rossby number would be $Ro = P_{\mathrm{rot}}/\tau_{\mathrm{conv}} \approx 0.13$. These values indicate quite high activity, being one order of magnitude smaller than the solar value ($Ro \approx 2$), although Ro for the most active stars might be still slightly smaller.

Stellar parameters of V889 Her, some of which are used in this analysis, are shown in table (4.1). A CCD image of the star, taken from the Metsähovi Observatory in Kirkko-

nummi, Finland, is shown in figure (4.1).

Table 4.1: Stellar parameters of V889 Her.

Parameter	Value	Referece
Right Ascension (J2000)	18h 34m 20.1s	(Gaia Collaboration et al., 2016)
Declination (J2000)	18° 41' 24.2"	(Gaia Collaboration et al., 2016)
Mean V-magnitude	7.46	(Kazarovets and Samus, 1997)
Spectral class	G2 V	(Montes et al., 2001)
Parallax	0.02629"	(van Leeuwen, 2007)
Distance	38 pc	Calculated from the parallax above
Inclination	60°	(Marsden et al., 2006)
$v \sin i$	38.5 km/s	This study
Age	30-50 Myr	(Strassmeier et al., 2003)
Mass	$1.06 \pm 0.02 M_{\odot}$	(Strassmeier et al., 2003)
Radius	$1.09 \pm 0.05 R_{\odot}$	(Strassmeier et al., 2003)
Metallicity ($Fe/Fe_{\odot}$)	-0.5	(Strassmeier et al., 2003)
Period	1.33697 d	(Järvinen et al., 2008)
α	0	(Huber et al., 2009)
Microturbulence	1.6 km/s	(Järvinen et al., 2008)
Macroturbulence	3.0 km/s	(Strassmeier et al., 2003)

4.1 Data

Both spectorscopic and photometric data have been used in the analysis. The spectroscopic data was obtained from the SOFIN high resolution spectrograph at the Norcid Optical Telescope at La Palma, Canary Islands, during 19th to 30th of July 2007. The photometric data comes from the T3 0.4m Automatic Photoelectric Telescope, located at Fairborn Observatory, Arizona. These data have been analysed using the Doppler imaging and CPS methods.

The photometric data is in the form of differential photometry, i.e. showing only

Figure 4.1: A CCD image of V889 Her (the brightest star in the image) in the V-band, taken on 10.4.2017 with the 60 cm Ritchey-Chrétien telescope in Metsähovi Observatory, Kirkkonummi, Finland.

the magnitude difference to a comparison star, HD 171286. This can be converted to an absolute magnitude scale when the magnitude of the comparison star, assumed to stay constant, is known. HD 171286 has a V-band magnitude $V = 6.84$ and a B-band magnitude $B = 7.90$ (Oja, 1987). V-band and B-band magnitudes for V889 Her, converted to the standard magnitude scale, are plotted in figure (4.2).

Some clear periodic changes can be seen in the magnitude of V889 Her, with a period of the order of a decade, and approximately two periods visible in the data. This would suggest an activity cycle similar to the solar cycle. What is also interesting, is that there seems to be a long-term trend of decreasing brightness. This could possibly be some change in the overall activity of V889 Her.

4.1.1 Doppler imaging

The spectroscopic data used for Doppler imaging was taken at the Nordic Optical Telescope in July 2007. Although the possible differential rotation would be an interesting issue to study, its effects are mostly not taken into account in this study, due to its complex nature and difficulties in accurately modelling it, since we cannot assume that it would necessarily follow an identical differential rotation law as the Sun (equation 2.6).

A spectral order of V889 Her is shown in figure (4.3). Three spectral regions with four significant absorption lines were combined in the analysis (these regions are shown in the lower panel of figure 5.1). These lines were the Fe I line at 641.16476 nm, Fe I

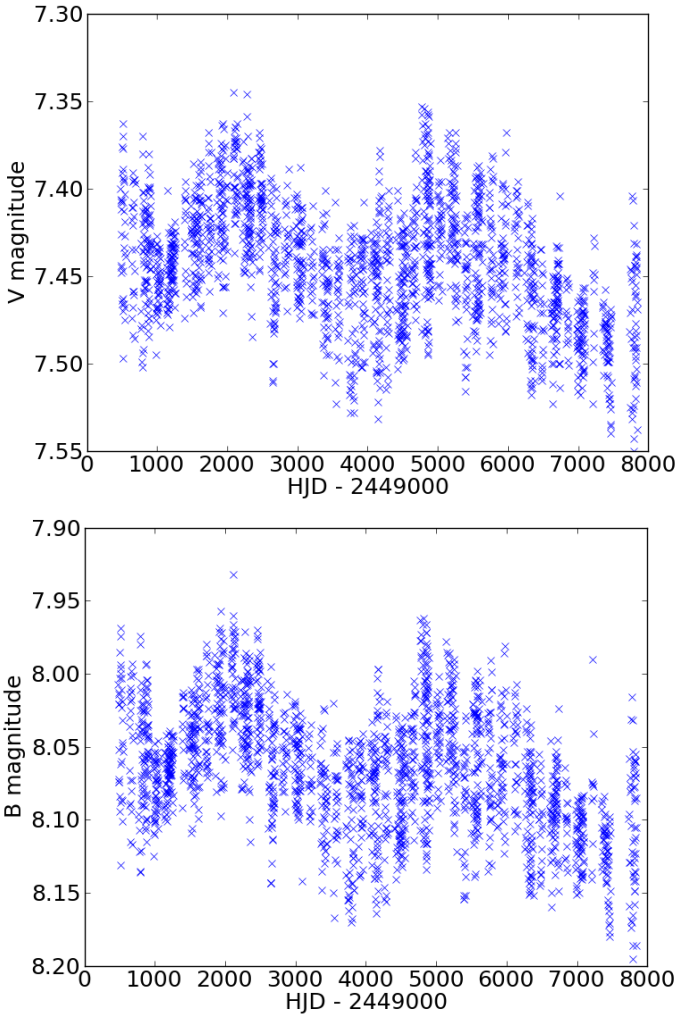

Figure 4.2: Upper panel: photometric V-band magnitudes for V889 Her. Lower panel: B-band magnitudes for V889 Her.

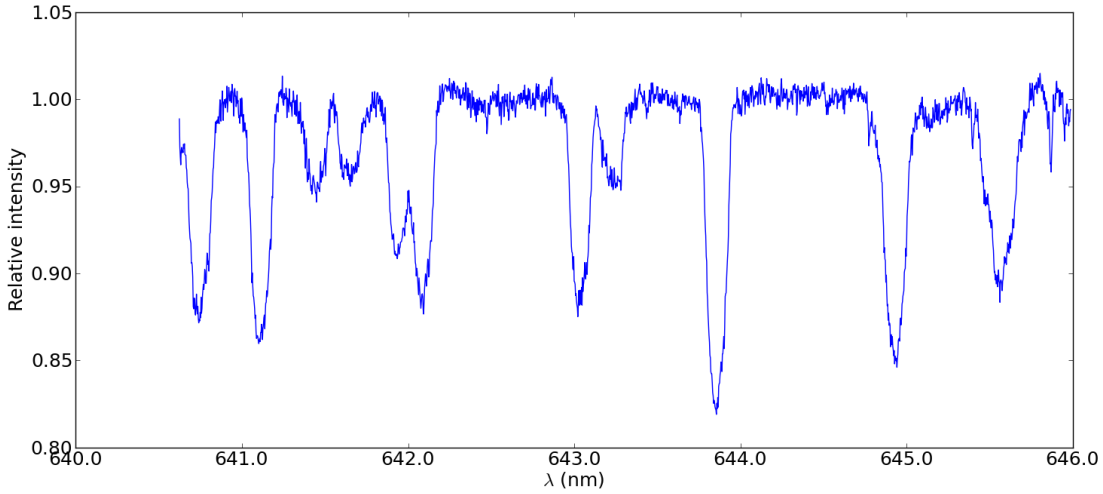

Figure 4.3: A spectral order of V889 Her.

line at 643.08446 nm, Fe II line at 643.26757 nm and Ca I line at 643.90750 nm. The surface temperature distribution of V889 Her was then fitted to these line profiles, using model atmospheres taken from MARCS[1] for the absorption properties at temperatures T = 3500 K, 3600 K,..., 3900 K, 4000 K, 4250 K, 4500 K,..., 6500 K. Allowed values for the temperature were thus between 3500 K and 6500 K. The program interpolates linearly between the given temperatures for the absorption properties of the model atmospheres, to gain a better temperature resolution. Before the temperature fitting, the spectra, initially reduced by the standard CCD reduction, were renormalized to the continuum level, by fitting a first order polynom to the continuum parts around the lines.

Different values for $v \sin i$ were tested around the previously reported values (e.g. Strassmeier et al. (2003) reported 39.0 km/s, Marsden et al. (2006) 37.5 km/s). The best fit, i.e. the value which minimizes the error function (equation 3.1) would be 38.0 km/s. In the final temperature map, $v \sin i$ was, however, chosen to be 38.5 km/s, even if the fit is slightly worse, because the temperature distribution appears smoother. With $v \sin i = 38.0$ km/s there appears to be stronger latitudal 'temperature bands', which are probably not real features (figure 5.2). All parameters used in the Doppler imaging procedure are listed in table (4.1).

[1] Available at marcs.astro.uu.se/index.php

4.1.2 Continuous Period Search

The photometric data used for the Continuous Period Search analysis spans for some 20 years, ranging from 1994 to 2014. Following the CPS procedure, the data has been divided into 55 independent sets and 39 segments. For sets with at least 10 data points the best period, mean magnitude and amplitude has been fitted, which allows us to follow the evolution of the phase of the minimum in each segment with enough datasets (which are not necessarily independent of each other). There is photometry of both V- and B-bands, which could be combined by assuming a linear correlation between them, as was done in Lehtinen et al. (2016). However, here only V-data has been used. This is reasonable, since there is plenty of V-band observations, so combining the V- and B-bands would not significantly improve the analysis, and no correlation has to be assumed.

There are periodic gaps in the data coverage due to seasonal changes in observing conditions. During each year, the observing period is interrupted by local sandstorms. The data is divided into segments accordingly.

In the CPS-analysis, the limiting order was set to $K_{\mathrm{lim}} = 2$, i.e. the model allows the fit to take into account orders of two or less in equation (3.3).

5. Results

5.1 Doppler imaging

The final Doppler map obtained from the spectral line profiles, with $v \sin i = 38.5$ km/s, is shown in figure (5.1). The most obvious, and only really certain, feature seen here is the large high latitude spot, which has also been reported by all previous Doppler imaging studies of V889 Her. This can be compared for instance with the Doppler map published by Frasca et al. (2010), whose data was taken about a year prior to that used in this thesis. An interesting feature appearing in the map of Frasca et al. (2010) is the smaller, secondary spot close to the major polar spot. This is not seen in the present map, which might indicate some notable changes in the spot configuration.

The temperature in the polar spot is around 4500 K, about the same temperature as sunspots. The temperature of the unspotted surface is also similar to that of the Sun, a little below 6000 K.

The spot filling factor was calculated by defining all surface elements of the Doppler map with a temperature $T < 5300K$ to be treated as spots. This choice of limiting temperature for spots is completely arbitrary, chosen just by estimating the temperature contours of the main spot. This gives a filling factor $f_S = 0.0345$. Even if there is only one spot resolved in V889 Her, this spot is still large enough to cause a spot filling factor notably larger than what would be expected in the Sun, although it is still quite far from the largest values (close to 0.5) derived for very active stars (e.g. O'Neal et al., 1998).

Small artefacts can be seen in the temperature map, which are probably not real features. There are no known physical reasons for vertical temperature 'stripes' or very strong latitudal temperature 'bands', such as in figures (5.2), (5.3), (5.4) and (5.5), with

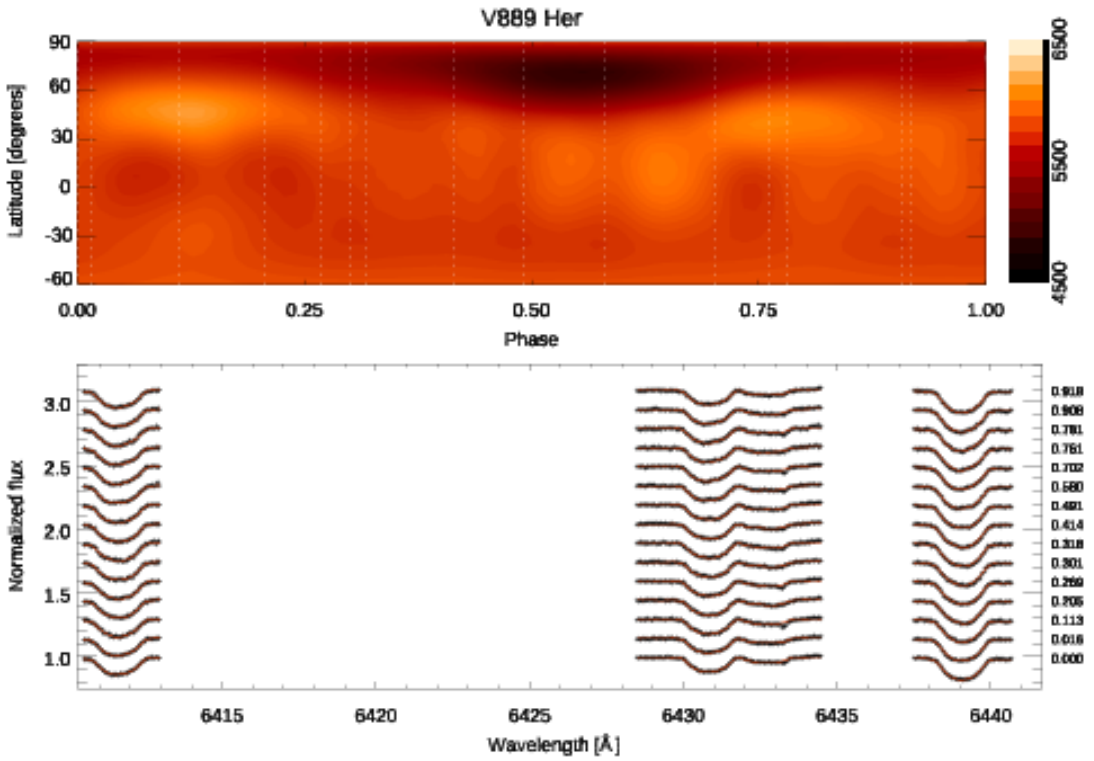

Figure 5.1: Upper panel: The final temperature map of V889 Her. The longitude has been converted to rotational phase, indicating which part of the star is facing the observer as the star rotates. The white vertical lines show the phases of the observed spectra. Lower panel: The three spectral regions used in the Doppler analysis. The model is shown in red, and the observations in black. Each spectra is shown in a relative flux scale, and shifted vertically by 0.1 from the previous one. The phase of each spectrum is shown on the right.

different values for $v \sin i$ and the differential rotation parameter α. In the final map, with $v \sin i = 38.5$ km/s and $\alpha = 0$, these features are still seen, but the overall distribution is smoother, which is the reason for choosing that value as the final one.

5.1.1 Differential rotation

To try to include differential rotation in the analysis, and to demonstrate its difficulties, the same procedure was repeated with inclusion of the differential rotation parameters $\alpha = 0.084$, $\alpha = 0.097$ and $\alpha = 0.105$ (equation 2.4), derived from values reported by Marsden et al. (2006) and Jeffers and Donati (2008). The resulting surface maps are shown in figures (5.3), (5.4) and (5.5). In all of these figures similar, very strong temperature bands

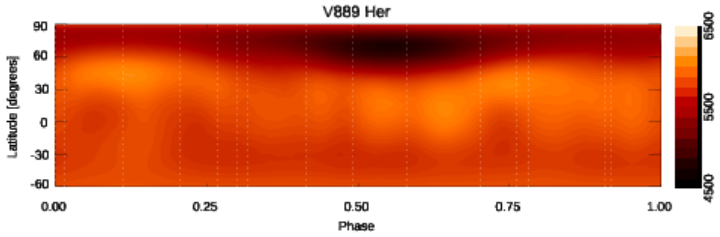

Figure 5.2: A temperature map of V899 Her for $v \sin i = 38.0$ km/s. This choise of $v \sin i$ causes stronger contours, for instance in latitudal temperature bands, than in figure (5.1).

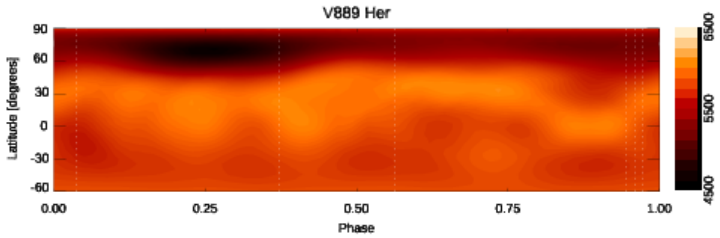

Figure 5.3: A temperature map of V889 Her with the differential rotation parameter $\alpha = 0.084$ taken from Marsden et al. (2006).

are seen. It is difficult to draw any definite conclusions from this, but the temperature map with no differential rotation seems a bit more reasonable. It demostrates, either way, the difficulties of studying differential rotation by Doppler imaging alone, since the current program does not search for the optimal value of α, but requires a given value as input. In the light of this study, a smaller value for α seems more likely. It is also notable, that in the situation with only one polar spot, differential rotation would not necessarily leave any marks to be found from photometry, because a spot covering more or less the whole latitudes around the pole, does not result in significant changes of the period, even if differential rotation would be present.

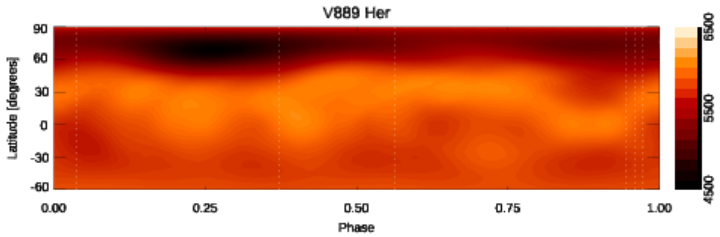

Figure 5.4: A temperature map of V889 Her with the differential rotation parameter $\alpha = 0.097$ taken from Jeffers and Donati (2008).

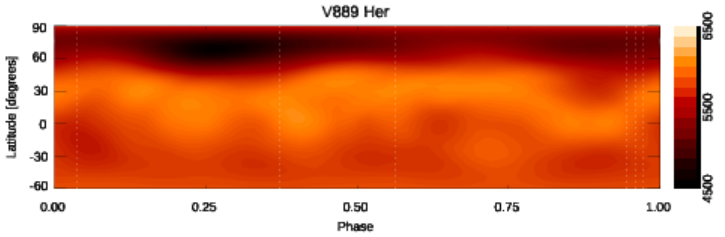

Figure 5.5: A temperature map of V889 Her with the differential rotation parameter $\alpha = 0.105$ taken from Jeffers and Donati (2008).

5.2 Photometry

Figure (5.6) shows the mean magnitude for each independent data set. The same periodicity is seen here as in the raw data. Figure (5.7) shows the best period for each independent set. After 2002 or so, this is not changing notably. In the late 1990's there are some sets with a longer period. One possible explanation for changes in the period could be spots on varying latitudes in a differentially rotating star. In figure (5.7) one can see that in July 2007, when the spectra used for Doppler imaging were taken, the period is very stationary. This is consistent with the Doppler map (figure 5.1) showing no lower latitude spots. At this time, the star is very close to its activity minimum, corresponding to luminosity maximum, assuming spot dominated luminosity variations (July 2007 is around HJD-2400000 = 54300). This is in agreement with the relatively simple spot configuration seen in the Doppler map, and might also explain the more complex configuration reported by Frasca et al. (2010), if the star had not yet reached its activity minimum when their spectra were taken, about a year prior to the data used here.

Figure (5.8) shows the amplitude for the magnitude variations in each independent set. The changes in the amplitude may correspond to changes in overall activity: the more active the star is, the more changes there are in the spot configuration, and the larger the amplitude should be. However, no clear dependences are seen in figure (5.8), the amplitude variations do not seem to follow the activity cycle. This could be interpreted as the spot configuration being relatively stationary, clearly the large polar spot is present even at the states of low activity. Even if the spots cover a larger area during high activity states, leading to suppressed brightness, the rotational variations are fairly similar throughout

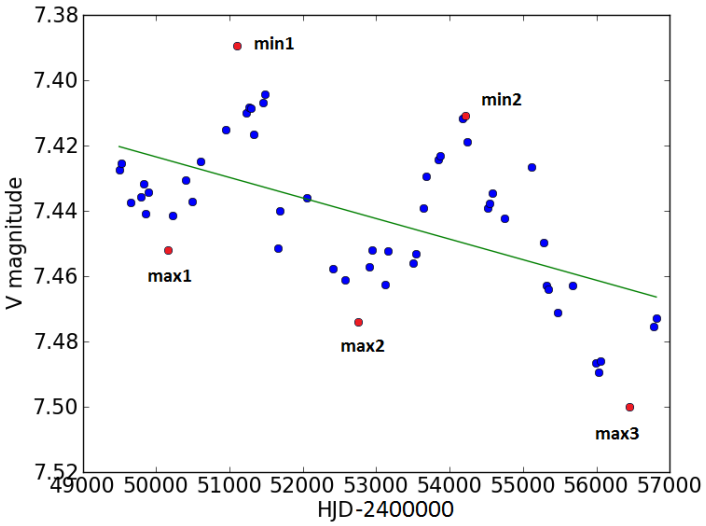

Figure 5.6: The mean magnitude for each independent set in the CPS analysis. The green line shows a linear fit used to remove the decreasing trend. The plot covers the time from 1994 to 2014. The sets defined as activity maxima and minima are marked as red.

the cycle.

5.2.1 Individual segments

The most interesting segments in the data, chosen to be presented more in detail, are segments 7, 21, 23 and 35. Figure (5.9) shows the evolution of the phase of the photometric minimum for these. Filled, black data points mark sets which are considered reliable, while open, white data points are unreliable (see section 3.2.1 for the definitions of these). Squares indicate primary minima, while triangles mark secondary minima. The number of the segment is shown in the upper right corner of each plot.

The photometric minimum occurs when the largest active region covers the largest part of the disk we see. In the selected segments there can be seen multiple minima, corresponding to multiple active regions on different longitudes.

In segment 7 the behaviour of the phase of the minimum is very erratic. The dominating longitude seems to move very rapidly, in 10 days or so, across the whole star. This is probably not a real feature, but caused by some rapid changes in the star, which leads to a wrong estimate for the period, which again leads to an erronous behaviour of

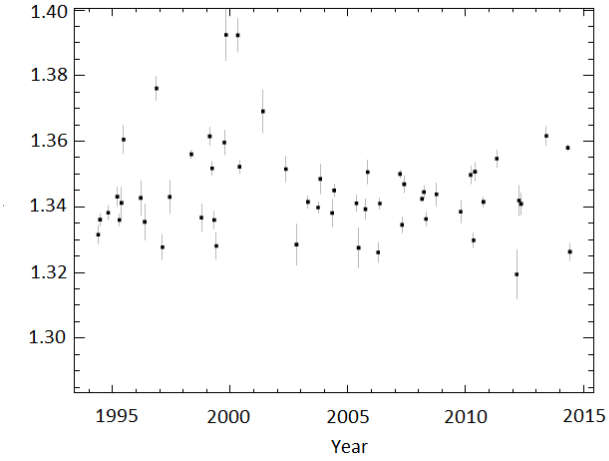

Figure 5.7: The best period for each independent set in the CPS analysis.

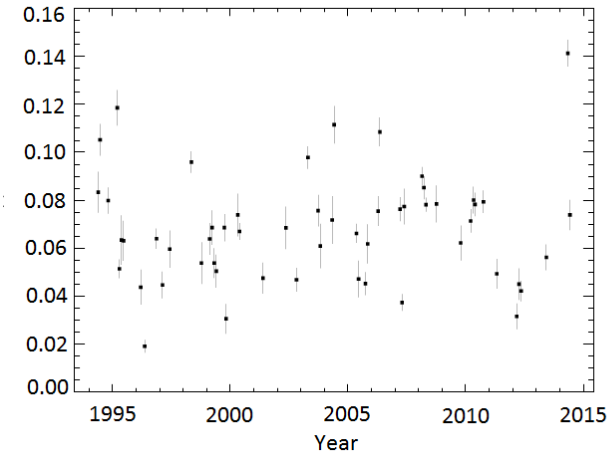

Figure 5.8: The best amplitude for each independent set in the CPS analysis.

the phase of the minimum. This also might happen, if the amplitude of the variations is too low to be reliably detected from the noise.

In segment 21 two active regions are separated by some 180 degrees (half a rotation) in the beginning of the data, before the secondary longitude fades out. This might indicate a flip-flop event. However, because of gaps in the data, nothing can be said about these active longitudes before the time period of this segment. If the fading active longitude would become dominating when going back in time, this would confirm the flip-flop, but with the existing data, this cannot be said for certain.

In segment 23 another, though even more uncertain flip-flop might take place, as the primary active longitude fades away and is replaced by the another one. They are separated by only about a third of the rotational phase, which is close to the maximum resolution that can be achieved to separate active regions (Lehtinen et al., 2011). The secondary minimum is also very weak, so it could be an error, which would mean there is really only the primary active region.

In segment 35 there appears again to be two active regions simultaneously, separated by some 180 degrees, but no clear shift is seen between them.

In all these segments, the star is close to its activity maximum, or luminosity minimum. This can be seen when comparing the Julian dates shown in each plot to those in figure (5.6).

These segments can be compared to segments where the minimum seems to be very stationary, showing only one photometric minimum and no apparent changes. Such a situation is seen in segments 1, 10, 22 and 29, which are shown in figure (5.10). In segments 1 and 22, the star is fairly close to activity maximum, but in segments 10 and 29 it is very close to minimum. It appears, that the more dramatic changes tend to happen close to activity maxima, whereas a stationary situation can be reached both close to minima and maxima.

5.2.2 Activity cycle

One can clearly see some periodical variations on a decadal time scale in the photometry, suggesting an activity cycle similar in length to the solar cycle (this is seen both in figures

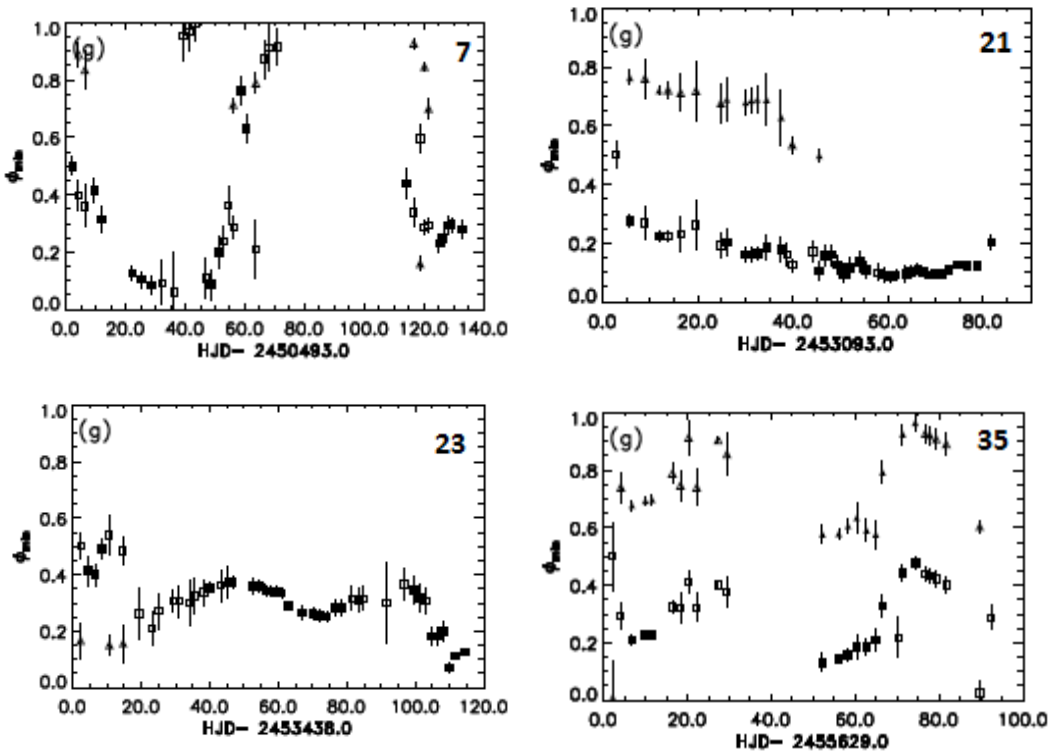

Figure 5.9: Results of the CPS analysis of the phase of the photometric minimum for segments 7, 21, 23 and 35, which all happen during high activity. Squares indicate the phase of the primary minimum, and triangles phase of the secondary minimum. Filled, black data points are considered reliable, while open, white data points are unreliable.

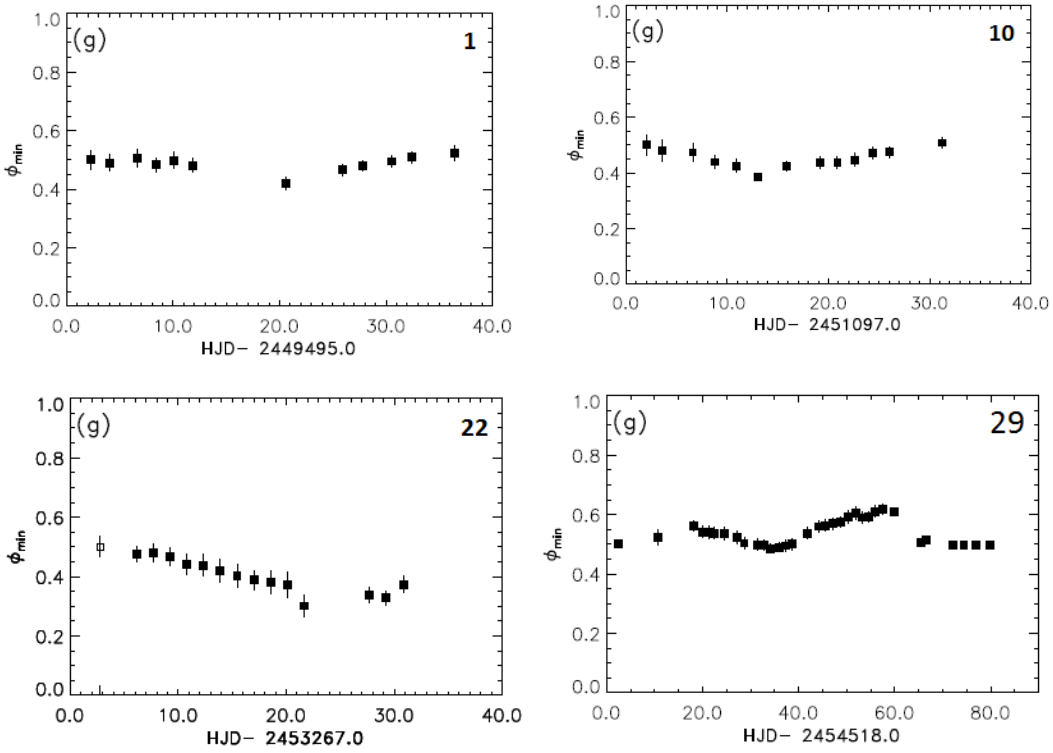

Figure 5.10: Same as figure 5.9 but for segments 1, 10, 22 and 29. Of these segments, 1 and 22 coincide with moderately high activity, whereas 10 and 29 are during low activity.

4.2 and 5.6). Interestingly, there is a decreasing trend in the brightness of the star between the cycles, which is also noted in the analysis of Lehtinen et al. (2016).

The power spectrum method was used to derive the best period for the activity cycle (equation 3.10). A linear fit was first made to the mean magnitudes for each independent set, which was then subtracted to remove the trend of increasing magnitude. The linear fit gave the result $M = 7.1088 + 6.2949 \cdot 10^{-6}$ HJD^{-1}t, where t is the Julian date of the observation. After the removal of this trend, the best period was found to be $P_{\rm cyc} = 9.81$ years, which is close to that reported by Lehtinen et al. (2016), as well as to the average length of the solar cycle.

In both cycles visible in the data, the phase of increasing activity would seem to be longer than the phase of decreasing activity. If the activity minimum and maximum are defined as the Julian date of the independent sets with the highest and lowest mean magnitude at the turnover points (these would be sets 8 (maximum 1), 14 (minimum 1), 26 (max 2), 38 (min 2) and 53 (max 3)), then the phases of decreasing activity would last for: $t_{\rm min1} - t_{\rm max1} = 942$ d and $t_{\rm min2} - t_{\rm max2} = 1461$ d, and the phases of increasing activity $t_{\rm max2} - t_{\rm min1} = 1652$ d and $t_{\rm max3} - t_{\rm min2} = 2238$ d. The defined starting and ending dates of these periods of rising and decaying activity (Julian dates of the sets marked in figure 5.6) are listed in table (5.1). If any conclusions can be drawn from these two cycles, this behaviour is different than that in the Sun, where the activity generally rises faster to its maximum, and takes longer time to decay to minimum. This could possibly be some sign of a different dynamo mechanism operating in V889 Her than in the Sun.

Also, the second cycle is longer than the first, so the best fit $P_{\rm cyc} = 9.81$ yr is not constant, but there are variations in the duration of the cycle, as there are in the Sun, too. The increasing cycle duration could perhaps be linked to the decreasing luminosity, but on the basis of only two cycles, not much can be said about it.

The decreasing trend in the luminosity of V889 Her could be explained by:

1) An increasing trend in the overall activity if V889 Her. This would predict the luminosity of the star to further decrease in the future.

2) Oscillations in the luminosity of V889 Her, depending on the cycle. This could be similar to the Gnevyshev-Ohl rule in the Sun, that the total sunspot number summed

Table 5.1: The start and end of the periods of decaying and rising activity. The duration of each phase is calculated as the difference between the end and start dates.

Phase of activity	Start (HJD)	End (HJD)	Duration (days)
Decay 1	2450157	2451099	942
Rise 1	2451099	2452751	1652
Decay 2	2452751	2454212	1461
Rise 2	2454212	2456450	2238

over an odd cycle is greater than that in the previous even cycle. This would predict the luminosity to increase in the next cycle.

3) Shift of activity between the hemispheres. This would require a hypothetical high latitude spot or active region near the pole invisible to us, fading away as the visible polar spot gets stronger. In that case no changes in the overall activity would be required. Although no evidence for this hypothesis exist, it could still be a possible explanation to the decreasing luminosity. In the Sun, activity is more or less symmetric on both hemispheres, but the situation does not necessarily have to be the same in V889 Her. Continuing with the hypothesis, even with more data, this situation would be difficult to distinguish from alternative (1) from photometry alone, but through continued Doppler imaging this hypothesis could be supported if the spot activity would increase only on polar areas, and not on lower latitudes, where spots would be visible on both hemispheres.

4) Random fluctuations. The existing data is not enough to exclude this possibility.

Figure (5.11) shows the B-V colour index of V889 Her. A similar periodicity can be seen here as in the magnitudes, corresponding to the activity cycle, although the variations are very small, only of the order of a few hundredths of a magnitude, while they are of the order of 0.1 magnitudes both in the V and B band. When comparing figure (5.11) to figure (4.2) or (5.6), one can see that the colour index anticorrelates with the luminosity during the activity cycle. This is reasonable, since when the luminosity is at minimum, the magnetic activity is at maximum, and so is the spottedness. The colour of the cold spots is redder than other parts of the photosphere.

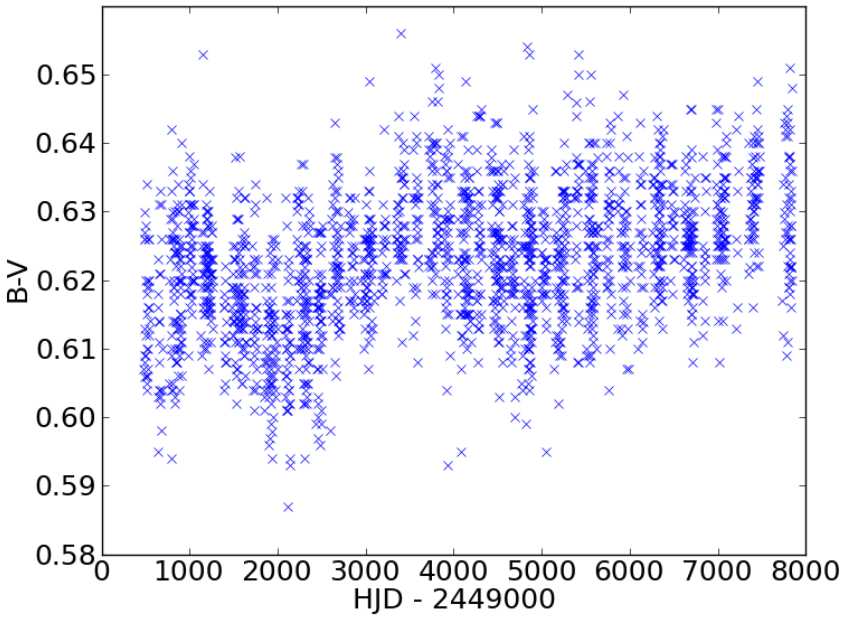

Figure 5.11: The colour index, B-V, of V889 Her as a function of time.

6. Conclusions

This Master's thesis has dealt with different forms of magnetic activity in the Sun and young, solar-like stars. The nature of the most important phenomena related to magnetic activity, especially those present in BY Draconis -stars, was reviewed in Chapter 2. This includes sunspots, starspots, (differential) rotation, the solar cycle and stellar cycles, the Gnevyshev-Ohl rule, the stellar dynamo, active longitudes and flip-flops. Other forms of magnetic activity, which cannot be studied using Doppler imaging or photometric time series analysis, including chromospheric activity, flares and Coronal Mass Ejections, were also discussed shortly. Chapter 2 also discussed the main properties of BY Draconis -stars, and the main stages of stellar evolution leading to stars as the present day Sun.

Chapter 3 described the methods used in studying active stars, Doppler imaging and time series analysis. The idea of Doppler imaging is to track temperature differences in a rotating star, as they affect the spectral line profiles. The Continuous Period Search was used for time series analysis, which is useful in identifying active longitudes and flip-flops, and studying cycle-to-cycle changes in the brightness, or the amplitude or period of the photometric variations.

Chapter 4 focused on one particular example of a young, solar-like star, V889 Herculis. This is a 7th magnitude star, classified as a BY Draconis -variable. It is a quite well studied star, with many previously published Doppler imaging maps existing. They all show a similar large high latitude spot. There are some inconsistent results about differential rotation. Some authors claim that V889 Her would show one of the highest measured values for differential rotation ever, while other studies have found no differential rotation at all. Also time series analysis has been done, showing clear variations in luminosity, of

the same time scale as the solar cycle.

Chapter 5 presented results of applying the methods from chapter 3 to V889 Her. The main result from spectral Doppler imaging is the confirmation of the high latitude polar spot, which is also found in all previously published Doppler images of the star. To include differential rotation, the analysis was also done using differential rotation values reported by Marsden et al. (2006) and Jeffers and Donati (2008). The resulting temperature maps, however, were deemed to be not as good as the one without differential rotation, because of unreasonable temperature bands. From this the conclusion can be drawn, that in light of the data used here, differential rotation could be completely absent in the star, or at least very inefficient. Although this is no strict evidence against differential rotation, it is what would usually be the expectation in these kinds of rapid rotators.

From the long-term photometry, the conclusion was drawn that the star was very close to its activity minimum (luminosity maximum) at the time when the spectra used in Doppler imaging were taken. This is supported by the relatively simple spot configuration, with only one large high latitude spot.

From the CPS-analysis, four interesting segments, all during high activity, were chosen for closer inspection. Out of these, one candidate for a flip-flop event was identified. To explain the increasing mean magnitude of V889 Her, four possible explanations were suggested: either an increase in the overall activity, a cycle-to-cycle variation similar to the Gnevyshev-Ohl rule in the Sun, the polar spot getting stronger without any global activity increase, or some random flucuations. By further observations of the following cycles, these explanations could be distinguished from each other. If the luminosity in the following cycle would further continue to decrease, this would favour the hypothesis of increasing activity, whereas if the luminosity would increase back to its previous level, this could be due to a similar effect as the Gnevyshev-Ohl rule. The situation with only the polar spot getting stronger would be difficult to distinguish from an overall increase in activity, because the other pole of the star remains hidden from us.

From all these phenomena, the conclusion can be drawn that although V889 Her and the Sun are similar in their mass and effective temperatures (both belong to the same spectral class G2 V), and both are single stars, the young age of V889 Her separates it

from the Sun in many ways. Some properties discussed in this thesis are presented for both these stars in table (6.1). Whereas sunspots are concentrated to low latitudes, the Doppler image shows a high latitude polar spot on V889 Her. This kind of spots have never been observed in the Sun, which strongly suggest that a different type of dynamo mechanism is behind the activity in V889 Her than the $\alpha\Omega$-dynamo in the Sun. This would probably be an $\alpha^2\Omega$ or α^2 -type of dynamo, where the role of differential rotation is less important. The rapid rotation, resulting in a low Rossby number, makes V889 Her magnetically much more active than the Sun, as is also suggested by the higher spot filling factor. Despite these differences, however, the length of the activity cycles are very similar. In contrast to the Sun, however, the phase of rising activity seems to last for a longer time than that of decaying activity, as deduced from the mean magnitudes.

To conclude, the young solar analogue is in many ways similar to the Sun, but shows strong signs of higher magnetic activity, as is expected of young stars, whose rotation has not yet slowed down. The activity is probably also sustained by a different type of dynamo than in the Sun. In the following billions of years, V889 Her is expected to lose most of its activity, and become more and more similar to the present day Sun. Studies of young solar-like stars can provide a more complete understanding of the relationship between the Sun and its young counterparts. This would also help us understand changes happening in the Sun, both in the past and in the future.

Table 6.1: Comparison of some parameters of the Sun and V889 Her.

Parameter	The Sun	V889 Her
Ro	~2	0.13
$f_{\rm s}$	< 0.003	0.0345
$P_{\rm rot}$ (measured at the equator)	~25 d	1.33697 d
$P_{\rm cyc}$	~11 yr	9.81 yr
Cycle phases	Fast rise, slow decay	Slow rise, fast decay
Spectral class	G2 V	G2 V
Dynamo type	$\alpha\Omega$	$\alpha^2\Omega$ / α^2

Bibliography

Aschwanden, M. J., Poland, A. I., and Rabin, D. M. The new solar corona. *Annu. Rev. Astron. Astrophys.*, 39:175, 2001.

Berdyugina, S. V. and Usoskin, I. G. Active longitudes in sunspot activity: Century scale persistence. *Astron. Astrophys.*, 405:1121, 2003.

Berdyugina, S. V. Starspots: A key to the stellar dynamo. *Living Rev. Solar Phys.*, 2:8, 2005.

Bopp, B. W. and Fekel, F. J. Binary incidence among the BY Draconis variables. *The Astronomical Journal*, 82:490, 1977.

Bouvier, J. Rotation in pre-main sequence stars: properties and evolution. In Catalano, S. and Stauffer, J. R., editors, *Angular Momentum Evolution of Young Stars*, volume 340 of *Mathematical and Physical Sciences*, page 41. Kluwer Academic Publishers, 1991.

Bruls, J., Solanki, S., and Schüssler, M. Doppler imaging: the polar spot controversy. *Astron. Astrophys.*, 336:231, 1998.

Byrne, P. B. On the believability of polar spots. In Strassmeier, K. G. and Linsky, J. L., editors, *Stellar Surface Structure*, volume 176 of *IAU Symposium*, page 299, 1996.

Callebaut, D., Makarov, V., and Tlatov, A. Monopolar structure of the Sun in between polar reversals and in Maunder Minimum. *Advances in Space Research*, 40:1917, 2007.

Chugainov, P. On the variability of HD234677. *Information Bulletin on Variable Stars*, 122, 1966.

Clayton, D. D. *Principles of Stellar Evolution and Nucleosynthesis*. The University of Chicago Press, 1983.

Deutsch, A. J. Harmonic Analysis of the Periodic Spectrum Variables. In Lehnert, B., editor, *Electromagnetic Phenomena in Cosmical Physics*, volume 6 of *IAU Symposium*, page 209, 1958.

Duric, N. *Advanced Astrophysics*. Cambridge University Press, 2004.

Faulkner, J., Roxburgh, I. W., and Strittmatter, P. A. Uniformly rotating main-sequence stars. *ApJ*, 151:203F, 1968.

Fleck, R. C. J. and Clark, F. O. A turbulent origin for the rotation of molecular clouds. *ApJ*, 245:898, 1981.

Fossat, E., Boumier, P., Corbard, T., Provost, J., Salabert, D., Schmider, F. X., Gabriel, A. H., Grec, G., Renaud, C., Robillot, J. M., Roca-Cortés, T., Turck-Chieze, S., Ulrich, R. K., and Lazrek, M. Asymptotic g-modes: Evidence for a rapid rotation of the solar core. *Astron. Astrophys.*, 604:A40, 2017.

Frasca, A., Biazzo, K., Kővári, Z., Marilli, E., and Çakırlı, Ö. Photospheric and chromospheric activity on the young solar-type star HD 171488 (V889 Herculis). *Astron. Astrophys.*, 518:A48, 2010.

Gaia Collaboration, Brown, A. G. A., Vallenari, A., Prusti, T., de Bruijne, J. H. J., Mignard, F., Drimmel, R., Babusiaux, C., Bailer-Jones, C. A. L., Bastian, U., et al. Gaia Data Release 1. Summary of the astrometric, photometric, and survey properties. *Astron. Astrophys.*, 595:A2, 2016.

Gnevyshev, M. N. and Ohl, A. I. On 22-year cycle of the solar activity. *Astron. Zh.*, 25: 18, 1948.

Goncharskii, A. V., Stepanov, V. V., Kokhlova, V. L., and Yagola, A. G. Reconstruction of local line profiles from those observed in an AP spectrum. *Sov. Astron. Lett.*, 3:147, 1977.

Gray, D. F. *The Observation and Analysis of Stellar Photospheres.* Cambridge University Press, 2005.

Hackman, T., Lehtinen, J., Rosén, L., Kochukhov, O., and Käpylä, M. J. Zeeman-Doppler imaging of active young solar-type stars. *Astron. Astrophys.*, 587:A28, 2016.

Hale, G. E. On the probable existence of a magnetic field in sun-spots. *ApJ*, 28:315, 1908.

Hale, G. E. and Nicholson, S. B. The law of sun-spot polarity. *ApJ*, 62:270, 1925.

Hall, J. C. Stellar chromospheric activity. *Living Rev. Solar Phys.*, 5:2, 2008.

Henry, G. W., Fekel, F. C., and Hall, D. S. An automated search for variability in chromospherically active stars. *The Astronomical Journal*, 110:2926, 1995.

Hoyt, D. V. and Schatten, K. H. Group sunspot numbers: A new solar activity reconstruction. *Sol. Phys.*, 179:189, 1998.

Huber, K. F., Wolter, U., Czesla, S., Schmitt, J. H. M. M., Esposito, M., Ilyin, I., and González-Pérez, J. N. Long-term stability of spotted regions and the activity-induced Rossiter-McLaughlin effect on V889 Herculis. *Astron. Astrophys.*, 501:715, 2009.

Jeffers, S. V. and Donati, J.-F. High levels of surface differential rotation on the young G0 dwarf HD 171488. *Mon. Not. R. Astron. Soc.*, 390:635, 2008.

Jetsu, L. and Pelt, J. Three stage period analysis and complementary models. *Astron. Astrophys. Suppl. Ser.*, 139:629, 1999.

Jetsu, L., Pelt, J., and Tuominen, I. Spot and flare activity of FK Comae Berenices: long-term photometry. *Astron. Astrophys.*, 278:449, 1993.

Järvinen, S. P., Korhonen, H., Berdyugina, S. V., Ilyin, I., Strassmeier, K. G., Weber, M., Savanov, I., and Tuominen, I. Magnetic activity on V889 Herculis. *Astron. Astrophys.*, 488:1047, 2008.

Karttunen, H., Donner, C. J., Kröger, P., Oja, H., and Poutanen, M. *Tähtitieteen perusteet (5. edition).* Tähtitieteellinen yhdistys Ursa ry, 2010.

Kazarovets, E. V. and Samus, N. N. The 73rd name-list of variable stars. *Information Bulletin on Variable Stars*, 4471, 1997.

Korhonen, H., Berdyugina, S. V., Strassmeier, K. G., and Tuominen, I. The first close-up of the "flip-flop" phenomenon in a single star. *Astron. Astrophys.*, 379:L30, 2001.

Kővári, Z., Frasca, A., Biazzo, K., Vida, K., Marilli, E., and Çakırlı, Ö. Differential rotation on the young solar analogue V889 Herculis. In D. P. Choudhary, . K. G. S., editor, *Physics of Sun and Star Spots*, volume 273 of *IAU Symposium*, page 121, 2011.

Kron, G. E. A photoelectric study of the dwarf M eclipsing variable YY Geminorum. *ApJ*, 115:301, 1952.

Lehtinen, J., Jetsu, L., Hackman, T., Kajatkari, P., and Henry, G. The continuous period search method and its application to the young solar analogue HD 116956. *Astron. Astrophys.*, 527:A136, 2011.

Lehtinen, J., Jetsu, L., Hackman, T., Kajatkari, P., and Henry, G. Activity trends in young solar-type stars. *Astron. Astrophys.*, 588:A38, 2016.

Marsden, S. C., Donati, J.-F., Semel, M., Petit, P., and Carter, B. D. Surface differential rotation and photospheric magnetic field of the young solar-type star HD 171488 (V889 Her). *Mon. Not. R. Astron. Soc.*, 370:468, 2006.

Montes, D., López-Santiago, J., Gálvez, M. C., Fernández-Figueroa, M. J., De Castro, E., and Cornide, M. Late-type members of young stellar kinematic groups - I. single stars. *Mon. Not. R. Astron. Soc.*, 328:45, 2001.

Noyes, R. W., Hartmann, L. W., Baliunas, S. L., Duncan, D. K., and Vaughan, A. H. Rotation, convection, and magnetic activity in lower main-sequence stars. *ApJ*, 279: 763, 1984.

Oja, T. UBV photometry of stars whose positions are accurately known. V. *Astron. Astrophys. Suppl. Ser.*, 71:561, 1987.

Oláh, K., Kolláth, Z., Granzer, T., Strassmeier, K. G., Lanza, A. F., Järvinen, S., Korhonen, H., Baliunas, S. L., Soon, W., Messina, S., and Cutispoto, G. Multiple and changing cycles of active stars II. Results. *Astron. Astrophys.*, 501:703, 2009.

O'Neal, D., Neff, J. E., and Saar, S. H. Measurements of starspot parameters on active stars using molecular bands in échelle spectra. *ApJ*, 507:919, 1998.

Ossendrijver, M. The solar dynamo. *The Astron Astrophys Rev*, 11:287, 2003.

Pelt, J., Tuominen, I., and Brooke, J. Century-scale persistence in longitude distribution in the Sun and in silico. *Astron. Astrophys.*, 429:1093, 2005.

Piskunov, N., Tuominen, I., and Vilhu, O. Surface imaging of late-type stars. *Astron. Astrophys.*, 230:363, 1990.

Popper, D. M. A possible new flare star. *PASP*, 65:278, 1953.

Radick, R. R., Lockwood, G. W., and Baliunas, S. L. Stellar activity and brightness variations: A glimpse at the Sun's history. *Science*, 247:39, 1990.

Reiners, A. and Schmitt, J. H. M. M. Differential rotation in rapidly rotating F-stars. *Astron. Astrophys.*, 412:813, 2003.

Reinhold, T., Cameron, R. H., and Gizon, L. Evidence for photometric activity cycles in 3203 Kepler stars. *Astron. Astrophys.*, 603:A52, 2017.

Roettenbacher, R. M., Monnier, J. D., Korhonen, H., Aarnio, A. N., Baron, F., Che, X., Harmon, R. O., Kővári, Z., Kraus, S., Schaefer, G. H., Torres, G., Zhao, M., ten Brummelaar, T. A., Sturmann, J., and Sturmann, L. No Sun-like dynamo on the active star ζ Andromedae from starspot asymmetry. *Nature*, 533:217, 2016.

Rosén, L., Kochukhov, O., and Wade, G. A. First Zeeman Doppler imaging of a cool star using all four Stokes parameters. *ApJ*, 805:169, 2015.

Rosén, L., Kochukhov, O., Hackman, T., and Lehtinen, J. Magnetic fields of young solar twins. *Astron. Astrophys.*, 593:A35, 2016.

Rüdiger, G., Pipin, V., and Belvedere, G. Alpha-effect, helicity and angular momentum transport for a magnetically driven turbulence in the solar convection zone. *Sol. Phys.*, 198:241, 2001.

Salaris, M. and Cassisi, S. *Evolution of stars and stellar populations.* John Wiley & Song, Ltd, 2005.

Scargle, J. D. Studies in astronomical time series analysis. II. Statistical aspects of spectral analysis of unevenly spaced data. *ApJ*, 263:835, 1982.

Schrijver, C. J. and Title, A. M. On the formation of polar spots in Sun-like stars. *ApJ*, 551:1099, 2001.

Schwabe, M. Sonnenbeobachtungen im Jahre 1843. von Herrn Hofrath Schwabe in Dessau. *Astronomische Nachrichten*, 21:233, 1844.

Schüssler, M. and Solanki, S. K. Why rapid rotators have polar spots. *Astron. Astrophys.*, 264:13, 1992.

Semel, M. Zeeman-Doppler imaging of active stars. I. Basic principles. *Astron. Astrophys.*, 225:456, 1989.

Snodgrass, H. B. and Ulrich, R. K. Rotation of Doppler features in the solar photosphere. *ApJ*, 351:309, 1990.

Solanki, S. K. and Unruh, Y. C. Spot sizes on Sun-like stars. *Mon. Not. R. Astron. Soc.*, 348:307, 2004.

Stoica, P. and Selén, Y. Model order selection: A review of information criterion rules. *IEEE Signal Processing Magazine*, 21:36, 2004.

Strassmeier, K. G., Pichler, T., Weber, M., and Granzer, T. Doppler imaging of stellar surface structure. XXI. The rapidly-rotating solar-type star HD 171488 = V889 Hercules. *Astron. Astrophys.*, 411:595, 2003.

Strassmeier, K. Doppler imaging of stellar surface structure XI. The super starspots on the K0 giant HD12545: larger than the entire Sun. *Astron. Astrophys.*, 347:225, 1999.

Strassmeier, K., Rice, J., Wehlau, W., Hill, G., and Matthews, J. Surface features of the lower atmosphere of HD 82558(= LQ Hydrae). *Astron. Astrophys.*, 268:671, 1993.

Svalgaard, L. and Schatten, K. H. Reconstruction of the sunspot group number: The backbone method. *Sol. Phys.*, 291:2653, 2016.

Unruh, Y. C. and Collier Cameron, A. Does chromospheric emission mimic polar starspots in Doppler images? *Mon. Not. R. Astron. Soc.*, 290:37, 1997.

Usoskin, I. G., Solanki, S. K., and Kovaltsov, G. A. Grand minima and maxima of solar activity: new observational constraints. *Astron. Astrophys.*, 471:301, 2007.

Usoskin, I., Kovaltsov, G., Lockwood, M., Mursula, K., Owens, M., and Solanki, S. A new calibrated sunspot group series since 1749: Statistics of active day fractions. *Sol. Phys.*, 291:2685, 2016.

Usoskin, I. G. A history of solar activity over milennia. *Living Rev. Solar Phys.*, 10:1, 2013.

van Leeuwen, F. Validation of the new Hipparcos reduction. *Astron. Astrophys.*, 474:653, 2007.

Vaquero, J. M., Kovaltsov, G. A., Usoskin, I. G., Carrasco, V. M. S., and Callego, M. C. Level and length of cyclic solar activity during the Maunder minimum as deduced from the active-day statistics. *Astron. Astrophys.*, 577:A71, 2015.

Vida, K., Kriskovics, L., Oláh, K., Leitzinger, M., Odert, P., Kővári, Z., Korhonen, H., Greimel, R., Robb, R., Csák, B., and Kovács, J. Investigating magnetic activity in very stable stellar magnetic fields. Long-term photometric and spectroscopic study of the fully convective M4 dwarf V374 Pegasi. *Astron. Astrophys.*, 590:A11, 2016.

Vogt, S. S. and Penrod, G. D. Doppler Imaging of spotted stars - Application to the RS Canum Venaticorum star HR 1099. *PASP*, 95:565, 1983.

Vogt, S. S., Penrod, G. D., and Hatzes, A. P. Doppler images of rotating stars using maximum entropy image reconstruction. *ApJ*, 321:496, 1987.

Waite, I. A., Marsden, S. C., Carter, B. D., Petit, P., Donati, J. F., Jeffers, S. V., and Boro Saikia, S. Magnetic field on young, moderately rotating Sun-like stars - I. HD 35296 and HD 29615. *Mon. Not. R. Astron. Soc.*, 449:8, 2015.

Willamo, T., Usoskin, I. G., and Kovaltsov, G. A. Updated sunspot group number reconstruction for 1749-1996 using the active day fraction method. *Astron. Astrophys.*, 601: A109, 2017.

Wilson, O. C. Chromospheric variations in main-sequence stars. *ApJ*, 226:379, 1978.

Zolotova, N. V. and Ponyavin, D. I. The Gnevyshev-Ohl rule and its violations. *Geomagnetism and Aeronomy*, 55:902, 2015.